The circular RNA *circGlis3* protects against islet β-cell dysfunction and apoptosis during obesity

Yue Liu
China Pharmaceutical University
Yue Yang
China Pharmaceutical University
Chenying Xu
China Pharmaceutical University
Jianxing Liu
China Pharmaceutical University
Jiale Chen
China Pharmaceutical University
Bin Huang
China Pharmaceutical University
Wenjing Yan
China Pharmaceutical University
Yi Pan
China Pharmaceutical University
Yanfeng Zhang
China Pharmaceutical University
Stephen J Pandol
Cedars-Sinai Medical Center
Qiong Wei
Southeast University
Fangfang Zhang
China Pharmaceutical University
Ling Li
Zhongda Hospital Southeast University
Liang Jin (ljstemcell@cpu.edu.cn)
China Pharmaceutical University https://orcid.org/0000-0002-1954-4345

Article

Keywords:

Posted Date: January 12th, 2022

DOI: https://doi.org/10.21203/rs.3.rs-1204703/v1

Version of Record: A version of this preprint was published at Nature Communications on January 21st, 2023. See the published version at https://doi.org/10.1038/s41467-023-35998-z.

Abstract

The molecular link between obesity and β-cell decompensation that causes diabetes remains incompletely understood. Here we found that *circGlis3*, a circular RNA derived from *Glis3*, plays a critical role in islet β-cell compensation. *circGlis3* was increased in islets of obese mouse models and moderately diabetic individuals with compensated β-cell function by Quaking (QKI)-mediated splicing. Overexpression of *circGlis3* functions to restrain islet β-cell dysfunction and maintain β-cell mass in high-fat diet (HFD) fed mice and *Lepr*$^{db/db}$ mice. The cellular levels of *circGlis3* modulate both insulin synthesis and secretion and lipotoxicity-induced apoptosis, resulting in profound changes in β-cell compensation. In an obesity model, *circGlis3* promotes the synthesis and secretion of insulin by upregulating *NeuroD1* and *Creb1* through sponging *miR-124-3p*. In addition, we identified SCOTIN and fused in sarcoma (FUS) as interacting proteins using quantitative mass spectrometry. We demonstrated that the binding of SCOTIN to *circGlis3* regulated the apoptosis of β-cell. And more, FUS binding to *circGlis3* could decrease free *circGlis3* in cytoplasm and block mechanism of *circGlis3* via abnormal stable formation of stress granules (SGs) in hyperactive response to chronic stresses in obesity that is thought to contribute to the β-cell decompensation. These findings highlight a physiological role for circRNAs in compensation and indicate that modulation of *circGlis3* expression may represent a potential strategy to protect against islet β-cell dysfunction and apoptosis during obesity.

Introduction

Type 2 diabetes mellitus (T2DM) progresses from compensated insulin resistance to β-cell failure resulting in uncompensated hyperglycemia. Obesity is a major risk factor for the development of T2DM through the mechanism of insulin resistance [1]. Interestingly, about 80% obese humans do not develop T2DM but adapt to chronic insulin resistance by increasing β-cell mass and insulin secretion [2]. In contrast, obese humans with T2DM have an 60% deficit in β-cell mass and that the mechanism underlying this is increased β-cell apoptosis [3,4]. Therapeutic approaches designed to arrest apoptosis could be a significant new development in the management of T2DM, because this approach might actually reverse the disease to a degree rather than just palliate glycemia. However, the mechanism of preventing β-cell apoptosis in the compensatory stage remains unclear.

β-cell to adapt its mass and function during obesity is associated with alterations in the expression of protein-coding and non-coding transcripts [5]. We previously indicated that different types of non-coding RNAs, including microRNAs and long non-coding RNAs, were key players in the regulation of β-cell functions in compensatory [6–8]. However, the role of the newly discovered class of circRNAs remains to be elucidated. Based on transcriptome profiling studies of islets, thousands of islet-specific circRNAs have been identified in human pancreatic islets, most of them were also conserved in mouse islets [9]. The first circRNA studied in pancreatic islet cells is *ciRS-7/CDR1as*. Overexpression of *ciRS-7* in murine islet cells was found to increase insulin content and secretion [10]. In another investigation, Lisa Stol et al documented that *circHIPK3* expression was directly related to insulin exocytosis by co-expression with

genes critical for normal islet function, such as *Akt1*, *Slc2a2*, and *Mtpn* [11]. More recently, other circRNAs dysregulated in the islets of diabetic *Lepr*$^{db/db}$ mice were identified by high-throughput RNA sequencing [12]. Although these studies provide an important groundwork documenting the function of circRNAs in β-cell, how these circRNAs contribute to obesity-mediated β-cell dysfunction and apoptosis remains to be determined.

Here, we identify a circRNA enriched in islets, *circGlis3*, which originates from an exonic sequence of *Glis3*. We demonstrate that *circGlis3* is upregulated in the islets of genetic and dietary mouse models of obesity. Mimicking this increase in HFD-fed mice and older *Lepr*$^{db/db}$ mice resulted in promoting insulin secretion and alleviating β-cell apoptosis. Mechanistically, *circGlis3* enhances insulin transcription and secretion via sponging *miR-124-3p*, alleviates apoptosis by inhibiting Caspase3-dependent manner via binding pro-apoptotic protein Scotin. It is interesting to note that, upon continuously elevated glycemia, expression of *circGlis3* is upregulated by splicing protein QKI, and then the free copy of *circGlis3* is decreased by FUS, which accumulated in cytoplasmic when β-cell suffered excessive stress and decompensation. Collectively, *circGlis3* is obesity responsive and appears as an essential regulator of β-cell biology. The upregulation of *circGlis3* links β-cell to adapt its mass and function during obesity.

Results

circGlis3 is elevated in the islets of obese mouse models

To identify circRNAs potentially contributing to the development of obesity-associated disturbances in β-cell dysfunction and apoptosis, we performed global circRNAs expression profiling in pancreatic islets obtained from islets of two mouse models of obesity: HFD-fed mice compared to normal chow diet (NCD) fed mice and mice homozygous for the obesity *ob* mutation of the leptin (*Lep*$^{ob/ob}$) compared to wild type littermates. Theses obese mouse models are capable of long-term compensatory insulin hypersecretion and β-cell mass [13]. The body weight, blood glucose and insulin levels of these mice were listed in Figure S1A-F. Out of 3646 circRNA-specific probe sets, 2738 and 2534 circRNAs were detected in islets of NCD/HFD and control/*Lep*$^{ob/ob}$, respectively (Figure S1G and H). In the islets of HFD-fed mice, expression of 302 circRNAs was significantly altered compared to circRNAs in NCD controls, of which expressions of 130 circRNAs increased and those of 172 circRNAs decreased (selection criteria: Log2 fold change >2 or <-2, $p < 0.05$; Figure S1G, Table S1). In *Lep*$^{ob/ob}$ islets, expressions of 767 circRNAs were significantly changed, of which expressions of 413 circRNAs increased and expressions of 354 decreased (selection criteria: Log2 fold change >2 or <-2, $p < 0.05$; Figure S1H, Table S2). Amongst the differentially expressed circRNAs, 45.2% overlapped with recently published transcripts by RNA-seq (Table S3) [14].

The changes observed in the circRNA levels were confirmed by qRT-PCR analysis of the 20 most dysregulated circRNAs, including 10 up-regulated and 10 down-regulated ones. Nearly 90% of the results of qRT-PCR were consistent with those of RNA-seq, indicating that the results of the RNA-seq were credible (Figure S1I and J). We chose the circRNA, mmu_circRNA006170 (circBase ID:

mmu_circ_0000943, termed *circGlis3* in the subsequent study because its host gene is *Glis3*) for further study. The reasons were as follows: (1) *circGlis3* was one of the most abundant circRNAs of the differentially expressed ones according to its Reads Mean in our RNA-seq (Table S4). (2) *circGlis3* was enriched in pancreas, and was also detectable in spleen, lung and kidney where the expression was more than 10 times lower compared to that in the pancreas (Figure 1A). (3) *circGlis3* was significantly upregulated in pancreas of HFD-fed mice, although the *mGlis3* (mRNA of *Glis3*) and protein levels of GLIS3 were downregulated (Figure 1B and C) as previously reported [15]. This finding indicated that the higher expression of *circGlis3* in obesity was not simply a by-product of splicing and was suggestive of functionality.

Then, we measured the expression of *circGlis3* in the islets of $Lep^{ob/ob}$ mice aged from 4 to 12 weeks, and observed the increase of *circGlis3* expression at the beginning of 6-week of age with the onset of insulin resistance (Figure 1D). We also observed a similar increase of expression of *circGlis3* in the islets of mice treated with 15-week HFD and young $Lepr^{db/db}$ mice, while the *circGlis3* expression was significantly decreased accompanied by glucose raising (Figure 1E and F), all of which showed that this observation is not limited to one mouse model of obesity and insulin resistance. Expressive abundance of *circGlis3* was also increased in other tissues of obese mice compared to normal mice, such as in the kidney, liver, lung, and brain (Figure S1K and L), although to a lesser extent than that observed in the islets. We also compared *circGlis3* expression in primary islet versus exocrine glands isolated from normal mice, revealing that *circGlis3* expression was 4.5-fold higher in islets versus exocrine glands, indicating that islets represent the main source of *circGlis3* expression in pancreas (Figure 1G). Moreover, we quantified *circGlis3* expression in the sera of a cohort of human individuals, the results shown that human individuals with impaired glucose tolerance performed higher *circGlis3* levels generally (Figure 1H). Interestingly, *circGlis3* levels were significantly increased in human serum from obese and moderately diabetic individuals with compensated β-cell function, but the *circGlis3* expression decreased in decompensated stage (Figure 1I, the concrete data were listed in Table S6). Taken together, the expression of *circGlis3* in the islets was increased in dietary and genetic mouse models of obesity, as well as in the sera of overweight with insulin resistance human subjects.

Splicing factor QKI regulates formation of circGlis3

Mouse *circGlis3* derived from Exon3 (Chr19:28530873-28531986) of the *Glis3* gene (Gene ID: 226075; ENSMUSG00000052942) with a length of 1114 nt on chromosome 19 (Figure 2A). The sequence is consistent with circBase database annotation (http://www.circbase.org/). Sequencing analysis confirmed its back-spiced junctions (Figure 2B). There are more than 80% homologous between human *circGlis3* and mouse *circGlis3* (Fig S2A). Divergent primers and convergent primers for *circGlis3* and linear transcript were designed. The cDNA and genomic DNA (derived from MIN6 cells) was amplified and analyzed using agarose gel electrophoresis (Figure 2C). We then investigated the stability and localization of *circGlis3* in MIN6 cells. Resistance to digestion with RNase R exonuclease confirmed that this RNA specie is circular inform (Figure 2D). qRT–PCR analysis of nuclear and cytoplasmic *circGlis3*

and fluorescence *in situ* hybridization (FISH) against *circGlis3* demonstrated that the circular form of *Glis3* Exon3 preferentially localized in the cytoplasm (Figure 2E and F).

We next investigated the mechanism by which *circGlis3* is formed. Previous studies have shown that splicing factors may participate in regulating circRNA biogenesis [16]. We postulated that if a protein factor contributes to *circGlis3* biogenesis, it would also be regulated by obesity. Based on this hypothesis, we investigated the expression level of a candidate panel of splicing factors in the islets of HFD-fed mice. We found that the QKI increased in obese mice at mRNA and protein levels (Figure 2G and H), and its expression level was positively correlated with *circGlis3* (Figure 2I, the concrete data were listed in Table S6). We also got the same pattern in glucose and palmitate stimulated MIN6 cells (Figure S2B and C). The effect of ectopic expression of QKI on *circGlis3* formation was confirmed by qRT–PCR analysis (Figure 2J), the transfection efficiency as shown in Figure 2SD. QKI usually works as a dimer, capable of binding two well separated regions of a single RNA molecule and promotes the circle-forming exons into close proximity and circRNA biogenesis [17]. To estimate whether QKI binding sites in the Introns flanking the circRNA-forming Exons of *Glis3*, we referenced the experimental scheme from Conn SJ [18], and searched for sequences that match potential QKI response elements (QREs) in the vicinity of the QKI RIP-enriched regions. We obtained four instances of a bipartite motif that contains the sequence UAAY in conjunction with a relaxed version of the canonical QKI hexamer [17] as previously reported [19]. There are two putative elements that located on upstream and two are located on downstream of the circRNA-forming splice sites, as shown in Figure 2K. To assess whether QKI binds the *Glis3* pre-mRNA, we performed RNA-immunoprecipitation (RIP) assays, using qRT-PCR to quantify QKI occupancy within the Introns adjacent to the *circGlis3* forming Exon3 (Figure 2L, Figure S2E). Pull-down assay also confirmed the binding interaction between the sites (which in the Introns flanking of *Glis3* Exon3) and QKI protein (Figure 2M). Ectopic expression of QKI in MIN6 cells, and more RIP assays were used to evaluate that QKI expression levels changed the binding interaction between motif sites (QRE1&2, QRE3, QRE4) (Figure 2N-P, Figure S2F-H). Subsequently, mutation of the single putative binding sites individually had little effect on circRNA formation, but mutation of both members of the upstream pair and the downstream pair substantially reduced circRNA formation, mutation of all four sites was more effective (Figure 3Q). All these data indicate that QKI binds upstream and downstream of the circRNA-forming Exon3 in *Glis3* to promote *circGlis3* formation.

Upregulation of circGlis3 **promotes insulin transcription and alleviates β-cell apoptosis** in vitro.

To explore the potential role of *circGlis3* in regulating β-cell function, we used short hairpin RNA targeting knockdown of *circGlis3* (*sh-circGlis3*), which is a group of three shRNAs to knock down *circGlis3* in MIN6 cell and primary islets respectively, and a plasmid with scramble sequence (*sh-NC*) as control. In addition, an overexpression plasmid (*oe-circGlis3*) was used to upregulate *circGlis3*. MIN6 cells and primary islets were transfected with *sh-circGlis3*, *sh-NC*, *oe-circGlis3*, or empty vector (*pEx3ciR*) and then were collected at 48 h. The efficiency of knockdown and overexpression were about 60% and 40-fold, respectively (Figure S3A and B). *oe-circGlis3* significantly increased the mRNA for the insulin genes (*Ins1* and *Ins2*) (Figure 3A and B) and the insulin content (Figure 3C and D), while knockdown of *circGlis3* induced the

opposite result. Glucagon content was not affected by the change in *circGlis3* levels (Figure S3C). Next, we performed glucose challenge experiments using primary islets and MIN6 cells with knockdown or overexpression of *circGlis3*. Suppression of *circGlis3* expression decreased insulin secretion after exposure to high glucose (16.7 mM glucose), and insulin secretion was markedly increased after *circGlis3* overexpression (Figure 3E and F). To explain how upregulation of *circGlis3* promotes insulin production, we detected both mRNA and protein expression of selected transcriptional factors with well-established roles in insulin transcription including pancreatic and duodenal homeobox factor 1 (Pdx1), neurogenic differentiation factor 1 (NeuroD1), Nk6 homeobox 1 (Nkx6.1), cAMP responsive element binding protein 1 (CREB1), and v-maf musculoaponeurotic fibrosarcoma oncogene homologue A (MafA). *circGlis3* overexpression selectively increased CREB1 and NeuroD1 both in mRNA and protein levels (Figure 3G and H). However, neither the mRNA nor the protein levels of Pdx1, Nkx6.1 and MafA were affected by *circGlis3* ectopic expression (Figure S3D and E). These results suggest that events responsible for the increase in insulin content may take place at the transcriptional level.

To identify the effect of *circGlis3* on maintaining β-cell mass, we modified *circGlis3* expression in MIN6 cells. CCK-8 assay showed that cell proliferation was slightly affected by regulating *circGlis3* (Figure S3F), and Ki67 immunofluorescent staining also echoed this result (Figure S3G). *circGlis3* overexpression in MIN6 cells resulted in a striking reduction in palmitate-induced apoptosis, as assessed by annexin V staining and by counting the cells displaying nuclei, further suggesting that *circGlis3* upregulation acts as a resister of the obesity-induced apoptosis of β-cell (Figure 3I). Then we performed TUNEL assay in MIN6 cells and primary mice islets, even in primary human islets, the results shown that the downregulation of *circGlis3* resulted in a rise in the number of apoptotic cells, but overexpression of *circGlis3* shown the opposite results (Figure 3J-L). Furthermore, western blot indicated that apoptosis proteins were altered in abnormal *circGlis3* treated cells, consistent with the flow cytometric and TUNEL analysis. Suppression of *circGlis3* expression induced Cleaved-CASPASE 3 and BAX expression while decreased BCL-2 expression, overexpression induced the opposite result (Figure 3M). These findings indicate that the upregulation of *circGlis3* can alleviate β-cell apoptosis during obesity.

Overexpression circGlis3 **protects against β-cell dysfunction and apoptosis** in vivo.

To test whether overexpression of *circGlis3* can alleviate obesity-induced β-cell dysfunction *in vivo*, 1×10^{12} adeno-associated virus particles expressing *circGlis3* (*oe-circGlis3*) was injected into male C57BL/6 mice aged at 8 weeks via pancreatic ductal infusion, and then fed the mice with HFD over 16 weeks. The time pattern of *oe-circGlis3* injection and HFD feeding is shown in Figure 4A. We observed about 9-fold upregulation of islets *circGlis3* expression in mice that had received the *oe-circGlis3* compared to those receiving adeno-associated virus particles with empty vector (*oe-vector*) even 20 weeks after injection (Figure S4A). The expression level of *circGlis3* was not significantly changed in other organs (Figure S4B). *oe-circGlis3* treatment had no effect on cumulative energy intake (Figure S4C) and body weight (Figure S4D). Overexpression of *circGlis3* as well as had no effect on fasting glycemia, although it was slightly lower than that in the control mice (Figure S4E). However, the fasting blood glucose was lower in *circGlis3* overexpression mice after 3 months of HFD feeding (Figure S4F). Homeostatic model

assessment of insulin resistance (HOMA-IR) indices of mice overexpressing *circGlis3* were significantly decreased (Figure 4B). In accordance with this, glucose tolerance tests revealed an improvement of glucose tolerance upon *circGlis3* overexpression (Figure 4C), insulin sensitivity was also improved upon upregulation of *circGlis3* (Figure 4D). Moreover, we isolated islets of *oe-circGlis3* treated and control mice after 8- and 16-week HFD feeding and performed GSIS test. The results revealed that insulin release was both markedly improved in *oe-circGlis3* treated mice when islets exposed to 16.7 mM glucose (Figure 4E and F). CREB1 and NeuroD1 protein levels were also increased in *oe-circGlis3* treated mice (Figure 4G). Morphometric analysis of the pancreas section revealed that β-cell mass was 1.7-fold higher in *oe-circGlis3* treated mice than in control mice (Figure 4H). TUNEL assays were also performed after 8- and 20-week HFD feeding. Counts of TUNEL-positive β-cell were lower by 67% and 56% in *circGlis3* overexpression mice after 8- and 20-week HFD feeding respectively, as compared to control animals (Figure 4I).

To confirm the effect of *circGlis3* on β-cell protection, the same virus particles were injected into *Lepr*$^{db/db}$ mice aged at 4 weeks. We found that overexpression of *circGlis3* prevented the increase of blood glucose at 10-week of age (Figure 4J). Further investigations demonstrated that the activation of *circGlis3* led to decrease in the number of TUNEL-positive β-cell (Figure 4K) and maintain the β-cell mass (Figure 4L). Corresponding to the above results, the upregulation of *circGlis3* resulted in significantly decreased the Cleaved-CASPASE 3 and BAX expression while increased BCL-2 expression (Figure 4M). Collectively, these results indicate that overexpression of *circGlis3* in dietary and genetic mouse models of obesity results in improvement of β-cell function and inhibited to β-cell apoptosis.

circGlis3 **regulates insulin transcription by sponging** miR-124-3p

circRNAs may function as competing endogenous RNAs (ceRNAs) to sponge miRNAs, thereby modulating the derepression of miRNA targets and imposing an additional level of post-transcriptional regulation [14]. To identify the potential miRNA targets of *circGlis3*, in silico analysis was performed by using Starbase, miRand, RNAhybrid and Targetscan databases, and jointly predicted that 4 miRNAs may act as biological targets of *circGlis*3 (Figure 5A). According to the assumption of ceRNA, the expression of circRNA and miRNA should show a negative correlation [20]. We then tested the expression patterns of the above miRNA in the islets of *Lep*$^{ob/ob}$ mice and HFD-fed mice. There were three miRNAs (*miR-124-3p*, *miR-298-5p* and *miR-3104-3p*) decreased in the islets of obese mice as opposed to the expression of *circGlis3*, while another one (*miR-3113-5p*) increased (Figure 5B and C). Although the expression pattern of *miR-3104-3p* is opposite to *circGlis3*, it showed very low abundance and hardly detected by qRT-PCR. The direct binding between the high abundance miRNAs (*miR-124-3p* and *miR-298-5p*) and *circGlis3* was validated by affinity pull-down of endogenous miRNAs associated with *circGlis3* using *in vitro* transcribed biotin-labeled *circGlis3* sense or anti-sense and demonstrated via qRT-PCR analysis. First, the efficiency of the biotin-labeled *circGlis3* binding on beads was detected (Figure S5A). The biotin-labeled *circGlis3* sense in MIN6 cells was significantly captured endogenous *miR-124-3p* compared to blank (Beads) and *circGlis3* anti-sense (Figure 5D). However, it slightly enriched for *miR-298-5p* (Figure S5B). FISH analysis was also detected in MIN6 cells, we found that *miR-124-3p* was co-localized with *circGlis3* in the

cytoplasm (Figure 5E). Based on the above results we selected *miR-124-3p* with the highest enrichment into further studies.

The predicted binding sites of *miR-124-3p* to *circGlis3* were illustrated in Figure S5C. For further confirmation, we constructed a dual-luciferase reporter by inserting the wild type (WT) or mutant (MT) linear sequence of *circGlis3* into pMIR-REPORT luciferase vector. We found that overexpression of *miR-124-3p* reduced the luciferase activities of the WT reporter vector but not mutant reporter vector (Figure 5F). Moreover, RNA pull-down assay using biotin-labeled *miR-124-3p* was also performed. The result revealed that endogenous *circGlis3* was pulled down by *miR-124-3p*, whereas the negative control with a disrupting putative binding sequence failed to co-precipitate out *circGlis3* (Figure 5G). As expected, upregulation of *circGlis3* reduced the level of *miR-124-3p*, and knockdown of *circGlis3* increased the level of *miR-124-3p* (Figure. 5H). However, we found no significant difference in *circGlis3* levels after overexpression or suppression of *miR-124-3p* in MIN6 cells (Figure S5D). This data demonstrated that *miR-124-3p* bound to *circGlis3* but did not induce the degradation of *circGlis3*. All these data demonstrated that *circGlis3* physically associated with *miR-124-3p* and may function as a ceRNA.

To investigate whether *circGlis3* regulates β-cell function through sponging *miR-124-3p*, the rescue experiment was performed. Overexpression of *circGlis3* in MIN6 cell and primary islets resulted in upregulated *Ins1* and *Ins2* transcript, while overexpression of *miR-124-3p* abrogated this activation (Figure 5I and J, Figure S5E). The promotion effects of insulin secretion were also abolished by overexpression of *miR-124-3p* (Figure 5K and L). To validate whether *circGlis3* may function as ceRNAs to modulate the derepression of *miR-124-3p* targets and imposed an additional level of post-transcriptional regulation, prediction of target genes of *miR-124-3p* was performed by TargetScan, Starbase, miRDB and miRWalk. *Creb1* and *NeuroD1* were in the intersection of predictions, which functions as major islet specific transcription factors (Figure S5F). The predicted binding sites of *miR-124-3p* to *Creb1* and *NeuroD1* were illustrated in Figure S5G and H. Luciferase reporter assay was applied through pMIR-REPORT vector holding wild-type or mutant 3'-UTR of *Creb1* and *NeuroD1*, respectively. We found that overexpression of *miR-124-3p* reduced the luciferase activities of the WT reporter vector but not mutant reporter vector (Figure 5M and N), and the protein level also changed accordingly (Figure 5O). The restraint effect of *miR-124-3p* on *Creb1* and *NeuroD1* were reversed with the addition of *circGlis3 in vitro* (Figure. 5P and Q) and *in vivo* (Figure. 5R and S). However, palmitate-induced cell apoptosis induced via downregulation of *circGlis3* could not be reversed by inhibition of *miR-124-3p* (Figure S5I). Altogether, these results suggest that *circGlis3* regulates β-cell function by competitively binding *miR-124-3p*, while this interaction did not affect β-cell apoptosis.

circGlis3 Interacts with SCOTIN to prevent β-cell apoptosis

We next investigated the mechanisms by which *circGlis3* prevented β-cell apoptosis during obesity. In addition to sponging for miRNAs, circRNAs could also regulate the functionality of RNA-binding proteins through direct binding [21]. To investigate this possibility for *circGlis3*, we performed experiments in which we biotinylated the *circGlis3* through assays of *in vitro* transcription and cyclization reaction (Figure S6A

and B), pulled it down using anti-biotin beads, and subjected the pull-downs to mass spectrometry. Several proteins were identified from this analysis as the potent *circGlis3* interacting protein (Table S5). Among the top candidates identified, SCOTIN and FUS most sparked our interest (Figure 6A, Figure S6C and D). SCOTIN is a pro-apoptotic factor, which is induced upon DNA damage or cellular stress in a p53-dependent manner [22,23]. We hypothesized that *circGlis3* could arrest β-cell apoptosis through the modulation of the SCOTIN.

We further confirmed the interaction between *circGlis3* and SCOTIN by running additional independent experiments. First, we performed RIP assays, where we confirmed that endogenous *circGlis3* interacts with SCOTIN in MIN6 cells (Figure 6B). Second, we pulled down the endogenous SCOTIN by biotinylated probes specific for *circGlis3*, and subjected the pull-down product to western blot analysis to detect the SCOTIN protein (Figure 6C). Finally, we coupled the circFISH protocol for *circGlis3* visualization with an immunofluorescence staining for SCOTIN in MIN6 cells and islets, and results demonstrated that *circGlis3* co-localized with the SCOTIN in the cytoplasm (Figure 6D). Taken together, these complementary set of experiments consistently showed that endogenous *circGlis3* can interact with SCOTIN. These interactions take place mainly in the cytoplasm, where SCOTIN mostly reside.

Based on these findings, we then aimed to investigate the possibility that *circGlis3* could function through the regulation of SCOTIN. We found that the SCOTIN was increased in the islets of 20-week HFD and *Lepr*$^{db/db}$ mice (Figure 6E and F), as well as in MIN6 cell which incubated with palmitate and glucose (Figure S6E and F), indicating a increase expression of SCOTIN in obese conditions. However, ectopic expression of *circGlis3* has no effect on the transcription and translation of SCOTIN (Figure S6G). Overexpression of *Scotin* can induce β-cell apoptosis in MIN6 cells and primary islets, while upregulation of *circGlis3* abrogated this effect (Figure 6G and H). The change trend of apoptosis detected by flow cytometry is consistent with the results of TUNEL experiment (Figure 6I). Further investigations demonstrated that overexpression of *Scotin* in HFD treated mice led to largely increase in the number of TUNEL-positive β-cells compared with control, while upregulation of *circGlis3* abrogated this effect (Figure 6J). Of note, overexpression of *Scotin* induces apoptosis of β-cell accompanied by sequestration of *circGlis3* in the cytoplasm (Figure 6K), and increased the Cleaved-CASPASE 3 and BAX expression while decreased BCL-2 expression (Figure 7L). It suggests that *circGlis3* prevents β-cell apoptosis in a Caspase-dependent manner during obesity by interacting with SCOTIN and decreasing SCOTIN activity.

FUS sequestrates circGlis3 **to reduce its abundance in diabetes**

Finally, we attempt to explain why the expression level of *circGlis3* decreased when diabetes occurred and lost its protective effect on β-cells. As mentioned earlier, the production of *circGlis3* is regulated by QKI. However, the expression level of QKI did not decrease prominently with the occurrence of diabetes (Figure 7A and B, the concrete data were listed in Table S6). It suggests that there may be additional mechanisms to regulate the level of *circGlis3* in diabetes. Using RNA pull-down assay and mass spectrometry analysis as we previously mentioned, we identified FUS that were pulled down by biotinylated probes specific for *circGlis3*, but not by probes for anti-sense (Figure S7A). FUS is a 70kDa

RNA-binding protein with multiple functions, which can shuttle between the nucleus and cytoplasm in responses to stress [24,25]. Interestingly, we found that the mRNA and protein levels of FUS were slightly up-regulated in HFD treated mice (Figure 7C) and MIN6 cells stimulated by glucose and palmitate (Figure S7B and C). Consistent with the results of previous studies [26], FUS mainly appears in the cytoplasm under stress (Figure 7D). Western blot analysis with anti-FUS antibody indicated the existence of FUS within the *circGlis3* sense RNA probe pull-down samples in MIN6 cells (Figure 7E). Meanwhile, a RIP assay with FUS antibody showed that endogenous FUS directly bound to *circGlis3* in MIN6 cells (Figure 7F). Ectopic expression of *circGlis3* have no direct effect on transcription and translation of FUS (Figure S7D and E). However, we observed that overexpression of *Fus* reduced the free copies of endogenous *circGlis3* in MIN6 cells and primary islets (Figure 7G), and the efficiency of overexpression as shown in Figure S7F.

In order to verify the regulatory effect of FUS on the downstream of *circGlis3*, we designed a series of competitive inhibition experiments. We found that overexpression of FUS accompanied by palmitate stimulation could reverse the inhibitory effect of *circGlis3* on *miR-124-3p*, which was specifically reflected in the increase of *miR-124-3p* and the downregulation of its target genes (Figure 7H). Similarly, the combination of FUS and SCOTIN with *circGlis3* is also competitive. The results of SCOTIN-RIP showed that FUS overexpression could competitively inhibit the enrichment of *circGlis3* by SCOTIN in the presence of palmitate (Figure 7I), and accompanied with the increased of TUNEL-positive β-cells in HFD mice islets (Figure S7G). Conversely, after overexpression of *Scotin*, FUS combined with *circGlis3* also decreased (Figure 7J).

It has been identified that the nuclear protein FUS quickly assembles cytoplasmic Stress Granules (SGs) during cellular stress [24]. Zhang's results supported that palmitate may disrupt nucleocytoplasmic transport by inducing SGs formation [27]. We then immunostained normal MIN6 cells and NCD-fed mouse pancreatic tissue for *circGlis3* and FUS and found that normal condition caused dispersed distribution of FUS in cytoplasm and nucleus with a few SGs assembly (Figure S7H). Given that SGs assembly may restricted diffusion of mRNAs and ncRNAs [28], we checked whether decrease of *circGlis3* is recruited into SGs assembly of FUS in palmitate-stimulated MIN6 cells and 20-week HFD-fed mice pancreas. As shown in Figure 7K and L, upregulation of FUS accelerated the SGs formation (white arrows), and abolished the *circGlis3* expression in cytoplasm when *circGlis3* was over-expressed. The above results indicate that when diabetes occurs, FUS competes with *miR-124-3p* and SCOTIN to bind *circGlis3*, resulting in the decrease of *circGlis3* by restricting diffusion in cytoplasm via recruitment function of FUS-formed SGs.

Discussion

In the common progress of T2DM, β-cell adaptation is a major mechanism in preventing T2DM progression, and failed β-cell compensation predicts the onset of T2DM [29]. This chronic progressive pathological process of T2DM indicates that there is an ample time window between functional depletion of insulin in β-cells and β-cells demise [30]. The molecular basis underlying compensatory β-cell mass is

largely unknown. We find in rodents that β-cell mass expansion during obesity is associated with the up-regulating expression of *circGlis3*. In isolated pancreatic islets and MIN6 cells, we recapitulate the increased *circGlis3* level observed in obese mouse models by activating the QKI splicing. *circGlis3* is elevated in the islets of obese mouse models and resulted in protects against islet β-cell dysfunction and apoptosis, while it decreases via FUS-formed SGs when diabetes occurs. (Figure 8). These findings point to a major role for *circGlis3* in compensatory β-cell function and mass occurring during obesity.

To probe the possible causes of the changes in *circGlis3* expression detected in the islets of obese individuals, we find that a substantial contribution to the regulation of *circGlis3* production comes from the regulation of circularization by the splicing factor QKI. QKI (Quaking), which belongs to STAR family of KH domain containing RNA binding proteins, has been identified to regulate pre-mRNA splicing [31,32] and has been implicated in various diseases including diabetes. QKI can bind bipartite sequence motifs [19] on the same or separate RNA molecules and form dimerization via N-terminal Qua1 domain [17]. The majority of QKI binding action occurs within introns, which containing potential QKI response elements [33]. Consistent with a role in splicing, QKI is essential for enhanced production of many circRNAs [18,34] and now acts by binding to recognition elements within Introns, which in the vicinity of the *circGlis3* forming splice sites. Furthermore, mutation of QKI motifs is intercepted to induce *circGlis3* formation. Secondary structure within Glis3 pre-mRNA that brings the head and the tail of Exon 3 into close proximity has been shown to enhance *circGlis3* biogenesis. It is attractively possible that QKI enhances *circGlis3* biogenesis through drawing the circle-forming Glis3 Exon 3 into close proximity via the dimer structure which capable of binding two well separated regions of a single RNA molecule.

With continuously rising glycemia, *circGlis3* levels in islets or clinical serum samples are shown a trend of first increase and then decrease. Herein our data show that chronic lipotoxicity stress caused SGs of FUS assembly, it was observed that *circGlis3* co-located with FUS and was restrained in SGs. SGs are non-membrane bound assemblies formed by phase separation, component of SGs could comprise abundant non-translating mRNAs, mRNA-binding proteins, ribonucleoproteins and translation initiation factors [28]. The structures of SGs are highly dynamic [35], and the interior components exchange with the surrounding cellular content inconstantly [36]. As a type of non-membrane-bound compartment, SGs behave like condensed liquid phases of the cytoplasm or nucleoplasm [37], generally are formed when cell suffering stress responses such as oxidative stress, endoplasmic reticulum (ER) stress and viral infection, and modulating the stress response [38]. Studies suggest that preventing SGs formation may be a potential therapeutic strategy for treating obesity and T2DM. For example, saturated fatty acids acted as endogenous stressors and disrupted PDX1 nucleocytoplasmic transport through stimulating SGs formation in pancreatic β-cell [27], and over-stress led to cytoplasmic SGs formation. It is interesting to note that SGs contain both mRNAs and ncRNAs [28], more analysis of the SG transcriptome reveals that SGs-enriched mRNAs are significantly distinct from the mRNAs that are secreted, mitochondria-localized, or ER-localized [28,39]. It could be explained that mRNAs are restricted diffusion when mRNAs are embraced in SGs. However, there has been little work on the SGs capturing circRNA and the relationship between this dynamic behavior and the onset of disease.

FUS, as an RNA-binding protein, performs critical functions in transcription, pre-mRNA splicing, RNA processing, and DNA repair. FUS rapidly shuttles between liquid compartments in the nucleus and the cytoplasm depending on the type of reversible stress, but is predominantly localized to the nucleus in unstressed cells. The liquid-like compartments of FUS maintain the trade-off between functionality and risk of aggregation in cytoplasm [26]. Disease-linked stimulation on the FUS can accelerate this aberrant phase transition from liquid drops to insoluble solid aggregates [40]. Accumulation of insoluble FUS in the cytoplasm is initiated in SGs [41], and simultaneous depletion of FUS from the nucleus may elicit degenerative disease [26]. In the present study, we investigate that chronic lipid stress induced SGs formation of FUS in cytoplasm, and free *circGlis3* are located and restricted to SGs via mutual combination with FUS. Therefore, it is highly likely that FUS-formed SGs restrain *circGlis3* and result in cytoplasmic free *circGlis3* gradually decrease with β-cell decompensation which triggered by long-term obesity or diabetes. Then function and downstream signal transduction mechanisms of *circGlis3* can be suppressed.

We would like to reiterate that increase of *circGlis3* level in obesity-islets is beneficial to maintain β-cell compensation through enhancing β-cell function and inhibiting β-cell apoptosis. The results demonstrate that *circGlis3* increase insulin transcription and secretion in β-cells *in vivo* and *in vitro* through sponging endogenous *miR-124-3p*, resulting in increased NeuroD1 and CREB1 expression. It has been reported that *miR-124-3p* in β-cell was involved in pancreas development and glucose metabolism [42] via regulating downstream target genes *Foxa2*. And *miR-124-3p* is also hyper-expressed in diabetic human pancreatic islets and negatively regulates insulin secretion [43]. *miR-124-3p* regulates multiple target genes, bioinformatics analysis and experiments reveal that *NeuroD1* and *Creb1* are the target genes of *miR-124-3p*. *NeuroD1* is an insulin transcription factor, which enhance insulin production by targeting insulin promoter [6,44]. *Creb1* plays a central role in gluconeogenic regulation, lipid metabolism and insulin signaling pathways [45], and it was required for the maintenance of glucose homeostasis and activator of the gluconeogenic regulation program [46]. In addition, *Creb1* can be targeted by *miR-10a* and regulate glucose metabolism and insulin secretion in T2DM [47]. Notably, we show that *circGlis3*/ *miR-124-3p*/ *NeuroD1* and *Creb1* are involved in pathological changes of β-cell in response to obesity. Insulin transcription and secretion of β-cell under obesity conditions are strongly inhibited by *miR-124-3p*, and this inhibition is reversed when *circGlis3* over-expressed.

Another more mechanism, *circGlis3* decelerate pancreatic β-cell apoptosis in obesity mice by retarding the activation of Caspase 3 pathway via binding to pro-apoptosis factor SCOTIN. *Scotin* gene is directly transactivated by p53 which is a transcription factor that induces growth arrest or apoptosis in response to cellular stress. The majority of SCOTIN protein is localized to the endoplasmic reticulum, and can induce cell apoptosis in a Caspase 3-dependent manner [48]. It has been verified that β-cell apoptosis could be a major contributor to the development of β-cell decompensation in late stages of T2DM, with a reduction in β-cell mass of 25–50% at the time of diagnosis [49]. In additional, previous studies in T2DM patients revealed that increasing β-cell apoptosis resulted in low proliferation and reduced β-cell mass. Since the *circGlis3* and SCOTIN are both located in cytoplasm, *circGlis3* may inhibit activity of the pro-

apoptosis protein via binding to SCOTIN. Nevertheless, overexpression or knockdown of *circGlis3* have no significant influence on β-cell proliferation *in vivo* and *in vitro*. These results indicate that overexpression of *circGlis3* contributes to insulin transcription and secretion by suppressing *miR-124-3p*/ *NeuroD1* and *Creb1* pathway, and decreases cell apoptosis via suppression of Caspase3-depended pathway through binding and inhibiting activity of SCOTIN. But when β-cell suffered to chronic lipid stress, free *circGlis3* could be captured by FUS-formed SGs in cytoplasm, leading to inhibiting effect of downstream mechanism of *miR-124-3p* sponging and SCOTIN binding.

In conclusion, our study reveals an important role of *circGlis3* in the development of obesity-associated β-cell dysfunction. It is observed that overexpression of *circGlis3* upregulates insulin transcription and secretion, improves abnormal glucose tolerance and β-cell apoptosis. In brief, upregulation of *circGlis3* lengthen the β-cell compensated stage and delay T2DM process. Thus, we speculate that *circGlis3* might potentially represent a new diagnostic and therapeutic target for T2DM, adding a new dimension to the functional importance of circRNA regulation in diabetes mellitus.

Methods

RNA-Sequencing and Analysis

Total islet RNA (200 islets per group) was isolated using the RNeasy kit (Qiagen) and treated with RNase R to deplete the linear transcripts. RNA integrity was assessed by the Agilent 2100 Bioanalyzer System (Agilent Technologies). The raw reads were filtered by removing reads containing adapter, ploy-N and low-quality reads for subsequent analysis. The expression level of circRNAs was measured by “Transcripts Per Kilobase Million” (TPM) [50]. Differentially expressed circRNAs of samples without biology replicates sample were evaluated by Statistical algorithm developed by Audic and Claverie and False discovery rate (FDR) analysis [51] for multiple testing. Differentially expressed circRNAs of samples with biology replicates sample were analyzed using DESeq2 package [52] based on the negative binomial distribution test.

Serum Samples and Human Islet

Human islets were provided from Tianjin First Central Hospital. The purity human islets (>80%) were collected and cultured in CMRL-1066 medium (Corning), supplemented with 10% Human Serum Albumin (Baxter), 100 U/mL penicillin and 100 μg/mL streptomycin at 37°C in 5% CO_2.

The clinical serum and clinicopathological data were collected from the Zhongda Hospital, Affiliated to southeast University (Nanjing, China). All the patients enrolled in this study was considered obese (BMI > 25). The negative controls were represented by lean individuals (20 ≤ BMI≤ 25).

All human subjects provided informed consent. All human studies were conducted according to the principles of the Declaration of Helsinki, were approved by the Ethics Committees of the Department

Zhongda Hospital Southeast University (Nanjing, China, 2018ZDSYLL132-P01). The clinical features of the patients are listed in Supplement Table 6.

Animal Experiments

Male C57BL/6 (7–8 weeks old) and *Lepr*$^{db/db}$ (4-5 weeks old) mice were purchased from the Model Animal Research Center of Nanjing University. All mice were housed in groups of 3–5 animals per cage, reared under a 12-hour light and 12-hour dark cycle with free access to water. C57BL/6 J mice were fed either with a normal diet consisting of standard lab chow or with high fat diet (HFD) for 8 weeks (D12494, 60% energy from fat) at least 3 months to establish a T2DM model. All animal experiments were carried out in strict accordance with the guidelines and rules formulated by the animal ethics committee of China Pharmaceutical University (Nanjing, China). Permit Number: 2162326.

Pancreatic Intraductal Viral Infusion

Male C57BL/6 and *Lepr*$^{db/db}$ mice were injected with adeno-associated virus serotype 8 vector (AAV8)-MIP (Mouse Insulin1 promoter)-*circGlis3* (ViGene Biosciences) or lentiviral vector up-LV2N-mmu-*miR-124-3p*-Puro (Gene Pharma) or lentiviral vector up-LV-MIP-Fus-Puro (Corues Biotechnology) or with control virus. The viruses [10^{12} GCP/mL] were infused at 6 μL/min by pancreatic intraductal viral infusion as previously study [7,53].

Glucose and Insulin Tolerance Tests in vivo

After viral infusion 2 weeks, glucose and insulin tolerance tests were carried out in mice. After fasted blood glucose measured, intraperitoneal glucose tolerance testing (IPGTT) was performed by injection of 2 g/kg body weight of glucose (Sigma), and blood glucose were determined after 5, 15, 30, 60, 90 and 120 min. For intraperitoneal insulin tolerance test (IPITT), the mice were intraperitoneally injected with 1 U/kg body weight of insulin after 12h overnight fasting. Serum sample was separated from orbital venous blood at 0, 5, 15 and 30 min. Insulin level was detected using mice insulin ELISA kit (Crystal Chem) according to the manufacturer's instructions.

Isolation, Culture and Dissociation of mouse islets

Mouse islets were isolated using intraductal collagenase technique [7,54] and terminated the digestive process in KRBH balanced buffer (115 mM NaCl, 4.8 mM KCl, 2.5 mM $CaCl_2$, 1.2 mM $MgSO_4$, 1.2 mM KH_2PO_4, 20 mM $NaHCO_3$, and 16 mM HEPES; pH 7.4) containing 1% FBS, 2.5 mM glucose and 1% penicillin/streptomycin. Then islets were handpicked and incubated overnight in 1640 medium containing 10% FBS and 1% penicillin/streptomycin. After incubated overnight in 1640 medium, the islets were seeded in plates used for various experiments.

Insulin Secretion and Content Assay

30 islets per well were seed in 96-well plate and transfected with either overexpressed-*circGlis3* plasmid or *sh-circGlis3* using Lipo2000 according to the manufacturer's instructions. MIN6 cells were seed in 48-well

plate and transfected. For glucose-stimulated insulin secretion (GSIS), islets or MIN6 cells were incubated at 37°C for 2 h in KRBH balanced buffer containing 2.5 mM, or 16.7 mM glucose after pre-incubation with KRBH balanced buffer containing 2.5 mM glucose and 10% FBS for 4 hours. Supernatants were collected and measured by mice insulin ELISA kit according to the manufacturer's instructions. The insulin secretion level was normalized by the total cellular protein content. For insulin content, the islets and MIN6 cells were extracted with acid ethanol. The insulin concentration of the extraction was measured by mice insulin ELISA kit and normalized by the total cellular protein content. The protein contents of mouse islets or MIN6 cells were quantified by BCA kit (Vazyme).

HOMA-IR

The homeostasis model assessment method was used to calculate insulin resistance (HOMA-IR), as described by Johnson's [55]. The fasting plasma glucose and insulin concentrations are calculated as following: fasting plasma glucose (mmol/L) × fasting plasma insulin (mU/L) / 22.5.

Total RNA Isolation and Real-Time Reverse Transcription-PCR (qRT-PCR)

Total RNA was first extracted from cell lines or tissues by using TRIzol (Solarbio) based on the guidebook. For mRNA or circRNA amplification, the RNA was reverse transcribed into cDNA by reverse transcriptase kit (ABM). Real-time PCR was were conducted by a LC480 Light Cycler (Roche) with qPCR SYBR Green Master Mix (Vazyme). For circRNA amplification divergent primer sets were used.

For miRNA amplification, reverse transcriptional reaction and real-time PCR were performed using Hairpin-itTM miRNAs qPCR Quantitation Kit (Gene Pharma) according to manufacturer's instructions.

All miRNA and mRNA levels were normalized to the expression of small RNAs (*sno234* and *U6*) or mRNA (*Gapdh* and *β-Actin*), respectively. All the primers applied in the study were shown in Supplement Table 7.

RNase R digestion

Total RNA was either untreated (control) or treated with RNase R (4 U/ug) (Epicenter) in the presence of 1 × Reaction Buffer, and incubated for 20 min at 37°C. Then reverse transcription and qRT-PCR were performed as described in the RNA extraction and qRT-PCR section.

Culture of MIN6 cells

The murine insulin-secreting cell line MIN6 was cultured in DMEM-Glutamax medium (Invitrogen), supplemented with 15% fetal calf serum (Gibco), 1% penicillin/streptomycin (Gibco), and 50 μM β-mercaptoethanol (Sigma). The MIN6 cells tested negative for mycoplasma contamination. Culture plates were kept in a humidified incubator with 5% CO_2 at 37°C. For palmitate treatment, islets and MIN6 cells were incubated in 0.5 mM palmitate (Sigma). For glucose treatment, islets and MIN6 cells were incubated in 33.3 mM glucose.

Cell Transfection

Transfection of dissociated mouse islets or MIN6 cells was carried out using Lipofectamine 2000 (Invitrogen) for plasmids, shRNA, siRNA sequences and miRNA mimics. Plasmids, shRNA, siRNA sequences and miRNA mimics are listed in the Supplement Table 7. All assays were performed 48 h after transfection.

Isolation of Cytoplasmic and Nuclear Fractionation

MIN6 cells at least 10^8 were harvested and treated using PARIS™ KIT protein and RNA isolation system (Invitrogen) according to the manufacturer's instructions. β-Actin and U6 served as controls of cytoplasmic RNA and nuclear RNA, respectively.

CCK-8 Analysis

The proliferation of MIN6 cells was measured by the CCK-8 assay (Vazyme). 5×10^3 cells in 100 μL were incubated in 96-well plates and cultured in conditional medium. Each sample was assayed in triplicate. At 0, 12, 24, 48, 72 h, 10 μL CCK-8 reagent was added to each well and incubated at 37°C for 1 h. After incubation, the absorbance at 450 nm was measured using an automatic microplate reader (BioTek).

Apoptosis Analysis

For flow cytometric analysis, MIN6 cells were transfected and collected after 48 hours. Cell apoptosis were determined using an Annexin V/FITC Apoptosis Detection Kit (Beyotime) according to the manufacturer's instructions. The FITC and PI were detected at 488 nm and 630 nm. Data were analyzed by FlowJo v10 software.

For TUNEL staining, the DNA fragmentation of islets or MIN6 cells were determined by TUNEL assay kit (Beyotime). Islets or MIN6 cell were fixed in 4% paraformaldehyde at room temperature for 15 min, then washed with PBS for 3 times and permeabilized with 0.3% Triton-X for 15 min. After pre-incubated with blocking solution (1% BSA) for 1 h, rabbit anti-insulin (1: 200) was incubated at 4°C overnight and goat anti-rabbit Alexa Fluor 647 (1: 500) was incubated at 37°C for 1 h. The islets or MIN6 cells were treated with TUNEL staining and observed under LSM510 Zeiss confocal microscope (Zeiss).

Western Blot

The whole cell lysate and nuclear-protein fractions were isolated from tissues or cells using a protein extraction kit (Beyotime). The pancreas tissues, primary islets (200 islets per group) and MIN6 cells were ruptured with RIPA buffer (Beyotime) containing 1% PMSF (Sigma). The protein concentration was quantified by BCA kit (Vazyme). Protein samples were resolved by SDS-PAGE and transferred onto PVDF membranes. The membranes were blocked for 2 h with 5% skimmed milk and incubated overnight at 4°C with primary anti-bodies. After washing three times with TBST, membranes were incubated for 1 h with appropriate secondary anti-bodies and developed using chemiluminescent substrates. All the antibodies are listed in Table S8.

Fluorescence in Situ Hybridization (FISH)

To detect the subcellular location of circRNA and miRNA, the probe hybridization was performed overnight with *circGlis3* or *mmu-miR-124-3p* probes using the fluorescent in situ hybridization kit purchased from (Gene Pharma). Cy3-labeled *circGlis3* probes and FAM-labeled *mmu-miR-124-3p* probes were incubated. samples were analyzed on LSM510 Zeiss confocal microscope (Zeiss). The *circGlis3* probe for FISH was 5'- GCAAAA+TAACGGACCGTACACT+TGT -3'and the *miR-124-3p* probe for FISH was 5'-GGCAT+TCACCGCGTGCCT+TA -3'.

Immunofluorescence

MIN6 cells were fixed with 4% paraformaldehyde and pancreas sections were deparaffinized and retrieved tissue antigen. The cells and pancreas sections were permeabilized by 0.3% Triton X-100 for 15 min and blocked with 1% BSA at 37℃ for 1 h. After incubation with primary anti-bodies at 4°C overnight, the Alexa Fluor conjugated secondaries (Abcam) were added and incubated at 37°C for 1 h. The cell nuclei were stained with DAPI (Beyotime) for 10 min at room temperature. Images were obtained with LSM510 Zeiss confocal microscope (Zeiss). All the antibodies are listed in Table S8.

RNA-binding protein Immunoprecipitation Assay

RNA immunoprecipitation (RIP) experiments were performed by using the Magna RIP RNA-Binding Protein Immunoprecipitation Kit (Millipore) according to the manufacturer's instructions. Approximately 1×10^7 cells were pelleted and resuspended with an equal pellet volume of RIP Lysis Buffer (100 µL) plus protease and RNase inhibitors. The cell lysates were incubated with 5 mg of control mouse IgG or antibody coated beads with rotation at 4°C overnight, respectively. After treating with proteinase K, the immunoprecipitated RNAs were extracted by phenol-chloroform extraction.

RNA Pull-down Assay and Mass Spectrometry Analysis

RNA pull-down was performed using a Magnetic RNA-Protein Pull-Down Kit (Thermo). Briefly, cell lysates were prepared by ultrasonication in RIP buffer (150 mM KCl, 25 mM Tris (pH 7.4), 0.5 mM dithiothreitol, 0.5% NP-40, complete protease inhibitors cocktail and RNase inhibitors) and pre-cleared against streptavidin magnetic beads (Invitrogen). Invitro transcribed biotin-labelled RNA probes adsorbed to streptavid in magnetic beads were then incubated with cell lysates at 4°C for 4 h before washing five times in RIP buffer and elution in Laemmli sample buffer. Mass spectrometric analysis of RNA-binding protein samples was entrusted to shanghai applied protein technology co. ltd (Shanghai, China).

In Vitro **Transcription**

The DNA template used for *in vitro* synthesis of biotinylated *circGlis3* was generated by PCR. The forward primer contained the T7 RNA polymerase promoter sequence to allow for subsequent *in vitro* transcription. PCR products were purified using the DNA Gel Extraction Kit (Vazyme), and *in vitro* transcription was performed using Transcript Aid T7 High Yield Transcription Kit (Thermo) and RNA 3'

End Biotinylation Kit (Thermo) according to the manufacturer's instructions. RNA was subsequently purified by phenol-chloroform extraction. Primer sequences are shown in Supplement Table 7.

In Vitro **Cyclization**

In vitro cyclization of linear RNA was performed according to Qidong Li with minor adaptations [54]. To assemble pre-ligation complexes, both biotin-labelled and unlabeled linear RNA were incubated with indicated DNA splints (at molar ratio 1: 1.5) respectively at 90℃ for 2 min, followed cooling to room temperature over 15 min. Ligation to form circular RNA was then incubated with T4 DNA ligase (Takara) at 16℃ overnight. Next, treated by RNase R and DNase I at 37℃ for 30 min to degrade residual linear RNA and DNA. RNA was purified finally by phenol-chloroform extraction. Primers and DNA splint sequences are shown in Supplement Table 7.

Mutation of QKI Response elements (QREs)

We made some alterations on the basis of previous study [18]. Genomic regions comprising Glis3 Exon 3 two introns were synthesized (Tsingke Biotechnology) with wild QREs sequence or mutational QREs (1, 2, 3 and 4, individually and synthetically) approximately 500 bp from the splicing site of the central exon. These were cloned into pcDNA3.1 and transfected into MIN6 cells that had been transfected 24 h previous with control or overexpressed-QKI plasmid. Then RNA was isolated 24 h later with TRIzol and treated with RNase R (Epicenter), cDNA was reverse transcribed and qRT-PCR was used to analysis the ratio of *circGlis3* to *Glis3.*

Luciferase assay

The pMIR-REPORT vector (Promega) with full-length *circGlis3* or 3'-UTR of *Creb1* and *NeuroD1* were used for luciferase report assays. The binding sites of *miR-124-3p* in *circGlis3* or 3'UTR of *Creb1* and *NeuroD1* were mutated to acted as mutant vectors. MIN6 cells were plated at the concentration of 10,000 cells per well in 24-well plates and cultured overnight. The cells were then transfected with 0.6 μg DNA per well (0.5 μg construct promoter and 0.1 μg constitutive renilla expression plasmid as a control for transfection efficiency) and *miR-124-3p* mimics or inhibitors. Cells were harvested 24h after transfection and luciferase activities were measured using a dual-luciferase reporter assay system (Promega). Transfection data represent at least three independent experiments each performed in triplicates.

Quantification and Statistical Analysis

All cell and biochemical assays were repeated a minimum of three times with unequivocal results obtained. The experiments involving human samples and animal samples were repeated twice. Statistical analysis was carried out using SPSS 22.0 and GraphPad Prism 7 to assess the differences between experimental groups. Data were analysed by two-tailed Student's t-test for two groups, one-way ANOVA with Tukey's post-test for univariate comparisons, two-way ANOVA with Bonfer-roni's post-test for bivariate comparisons, or the Pearson coefficient for the linear correlation between two variables. Error

bars in the figure legends indicate the standard error of the mean (SEM). The statistical significance difference was set at $^{*}p < 0.05$, $^{**}p < 0.01$, and $^{***}p < 0.001$.

Declarations

Author Contributions

Y.L, Y.Y, JX.L, B.H and WJ.Y performed the experiments; Y.P and Y.F.Z analyzed data; Q.W, L.L, F.F.Z and L.J designed the project, Stephen J Pandol embellished the language of the manuscript. Y.L and L.J interpreted the data and wrote the manuscript.

Acknowledgments

This work was supported by National Natural Science Foundation of China (Grant No. 82070801, 82100858); Supported by grants from the '111' project (B16046); Supported by Priority Academic Program Development of Jiangsu Higher Education Institutions (PAPD); Supported by China Postdoctoral Science Foundation (2020M671661); Supported by Jiangsu Province Science Foundation for Youths (BK20200569); Supported by Jiangsu Province Research Founding for Postdoctoral (1412000016).

References

1. Tyrberg, B., Ustinov, J., Otonkoski, T. & Andersson, A. Stimulated Endocrine Cell Proliferation and Differentiation in Transplanted Human Pancreatic Islets. *Diabetes* **50**, 301–307 (2001).
2. Polonsky, K. Dynamics of insulin secretion in obesity and diabetes. *Int J Obes Relat Metab Disord* **Suppl 2**(2000).
3. Butler, A.E., *et al.* Beta-cell deficit and increased beta-cell apoptosis in humans with type 2 diabetes. *Diabetes* **52**, 102–110 (2003).
4. Butler, A.E., Janson, J., Soeller, W.C. & Butler, P.C. Increased β-Cell Apoptosis Prevents Adaptive Increase in β-Cell Mass in Mouse Model of Type 2 Diabetes. *Diabetes* **52**(**9**):**2304-14**(2003).
5. Guay, C., *et al.* Emerging roles of non-coding RNAs in pancreatic beta-cell function and dysfunction. *Diabetes Obes Metab* **14 Suppl 3**, 12–21 (2012).
6. Zhang, F., *et al.* Obesity-induced overexpression of miR-802 impairs insulin transcription and secretion. *Nat Commun* **11**, 1822 (2020).
7. Zhang, F., *et al.* The long non-coding RNA betaFaar regulates islet beta-cell function and survival during obesity in mice. *Nat Commun* **12**, 3997 (2021).
8. Zhang, F.F., *et al.* Obesity-induced reduced expression of the lncRNA ROIT impairs insulin transcription by downregulation of Nkx6.1 methylation. *Diabetologia* **63**, 811–824 (2020).
9. Stoll, L., *et al.* Circular RNAs as novel regulators of beta-cell functions in normal and disease conditions. *Mol Metab* **9**, 69–83 (2018).

10. Xu, H., Guo, S., Li, W. & Yu, P. The circular RNA Cdr1as, via miR-7 and its targets, regulates insulin transcription and secretion in islet cells. *Sci Rep* **5**, 12453 (2015).
11. Zheng, Q., *et al.* Circular RNA profiling reveals an abundant circHIPK3 that regulates cell growth by sponging multiple miRNAs. *Nat Commun* **7**, 11215 (2016).
12. Wu, L., *et al.* Circ-Tulp4 promotes beta-cell adaptation to lipotoxicity by regulating soat1 expression. *J Mol Endocrinol* **65**, 149–161 (2020).
13. Kleinert, M., *et al.* Animal models of obesity and diabetes mellitus. *Nat Rev Endocrinol* **14**, 140–162 (2018).
14. Memczak, S., *et al.* Circular RNAs are a large class of animal RNAs with regulatory potency. *Nature* **495**, 333–338 (2013).
15. Hall, E., *et al.* Effects of palmitate on genome-wide mRNA expression and DNA methylation patterns in human pancreatic islets. *BMC Med* **12**:**103**(2014).
16. Ashwal-Fluss, R., *et al.* circRNA biogenesis competes with pre-mRNA splicing. *Mol Cell* **56**, 55–66 (2014).
17. Teplova, M., *et al.* Structure-function studies of STAR family Quaking proteins bound to their in vivo RNA target sites. *Genes Dev* **27**, 928–940 (2013).
18. Conn, S.J., *et al.* The RNA binding protein quaking regulates formation of circRNAs. *Cell* **160**, 1125–1134 (2015).
19. Galarneau, A. & Richard, S. Target RNA motif and target mRNAs of the Quaking STAR protein. *Nat Struct Mol Biol* **12**, 691–698 (2005).
20. Piwecka, M., *et al.* Loss of a mammalian circular RNA locus causes miRNA deregulation and affects brain function. *Science* **357**(2017).
21. Patop, I.L., Wust, S. & Kadener, S. Past, present, and future of circRNAs. *EMBO J* **38**, e100836 (2019).
22. Gupta, R.K., Tripathi, R., Naidu, B.J., Srinivas, U.K. & Shashidhara, L.S. Cell cycle regulation by the pro-apoptotic gene Scotin. *Cell Cycle* **7**, 2401–2408 (2008).
23. Bourdon, J.C., Renzing, J., Robertson, P.L., Fernandes, K.N. & Lane, D.P. Scotin, a novel p53-inducible proapoptotic protein located in the ER and the nuclear membrane. *J Cell Biol* **158**, 235–246 (2002).
24. Castanotto, D., *et al.* A stress-induced response complex (SIRC) shuttles miRNAs, siRNAs, and oligonucleotides to the nucleus. *Proc Natl Acad Sci U S A* **115**, E5756-E5765 (2018).
25. Maharana, S., *et al.* RNA buffers the phase separation behavior of prion-like RNA binding proteins. *Science* **360**, 918–921 (2018).
26. Patel, A., *et al.* A Liquid-to-Solid Phase Transition of the ALS Protein FUS Accelerated by Disease Mutation. *Cell* **162**, 1066–1077 (2015).
27. Zhang, M., *et al.* Saturated fatty acids entrap PDX1 in stress granules and impede islet beta cell function. *Diabetologia* **64**, 1144–1157 (2021).
28. Khong, A., *et al.* The Stress Granule Transcriptome Reveals Principles of mRNA Accumulation in Stress Granules. *Mol Cell* **68**, 808-820 e805 (2017).

29. Prentki, M., Peyot, M.L., Masiello, P. & Madiraju, S.R.M. Nutrient-Induced Metabolic Stress, Adaptation, Detoxification, and Toxicity in the Pancreatic beta-Cell. *Diabetes* **69**, 279–290 (2020).
30. Talchai, C., Xuan, S., Lin, H.V., Sussel, L. & Accili, D. Pancreatic beta cell dedifferentiation as a mechanism of diabetic beta cell failure. *Cell* **150**, 1223–1234 (2012).
31. Hall, M.P., *et al.* Quaking and PTB control overlapping splicing regulatory networks during muscle cell differentiation. *RNA* **19**, 627–638 (2013).
32. Lee, J., *et al.* QUAKING Regulates Microexon Alternative Splicing of the Rho GTPase Pathway and Controls Microglia Homeostasis. *Cell Rep* **33**, 108560 (2020).
33. Hafner, M., *et al.* Transcriptome-wide identification of RNA-binding protein and microRNA target sites by PAR-CLIP. *Cell* **141**, 129–141 (2010).
34. Chen, D., *et al.* Targeting the radiation-induced TR4 nuclear receptor-mediated QKI/circZEB1/miR-141-3p/ZEB1 signaling increases prostate cancer radiosensitivity. *Cancer Lett* **495**, 100–111 (2020).
35. Aggarwal, S., *et al.* Myelin membrane assembly is driven by a phase transition of myelin basic proteins into a cohesive protein meshwork. *PLoS Biol* **11**, e1001577 (2013).
36. Wippich, F., *et al.* Dual specificity kinase DYRK3 couples stress granule condensation/dissolution to mTORC1 signaling. *Cell* **152**, 791–805 (2013).
37. Lee, C.F., Brangwynne, C.P., Gharakhani, J., Hyman, A.A. & Julicher, F. Spatial organization of the cell cytoplasm by position-dependent phase separation. *Phys Rev Lett* **111**, 088101 (2013).
38. Protter, D.S.W. & Parker, R. Principles and Properties of Stress Granules. *Trends Cell Biol* **26**, 668–679 (2016).
39. Chartron, J.W., Hunt, K.C. & Frydman, J. Cotranslational signal-independent SRP preloading during membrane targeting. *Nature* **536**, 224–228 (2016).
40. Murakami, T., *et al.* ALS/FTD Mutation-Induced Phase Transition of FUS Liquid Droplets and Reversible Hydrogels into Irreversible Hydrogels Impairs RNP Granule Function. *Neuron* **88**, 678–690 (2015).
41. Hofweber, M., *et al.* Phase Separation of FUS Is Suppressed by Its Nuclear Import Receptor and Arginine Methylation. *Cell* **173**, 706-719 e713 (2018).
42. Baroukh, N., *et al.* MicroRNA-124a regulates Foxa2 expression and intracellular signaling in pancreatic beta-cell lines. *J Biol Chem* **282**, 19575–19588 (2007).
43. Sebastiani, G., *et al.* MicroRNA-124a is hyperexpressed in type 2 diabetic human pancreatic islets and negatively regulates insulin secretion. *Acta Diabetol* **52**, 523–530 (2015).
44. Guo, S., *et al.* Inactivation of specific beta cell transcription factors in type 2 diabetes. *J Clin Invest* **123**, 3305–3316 (2013).
45. Herzig, S., *et al.* CREB regulates hepatic gluconeogenesis through the coactivator PGC-1. *Nature* **413**(**6852**), 179–183 (2001).
46. Chen, J., Zhang, C., Mi, Y., Chen, F. & Du, D. CREB1 regulates glucose transport of glioma cell line U87 by targeting GLUT1. *Mol Cell Biochem* **436**, 79–86 (2017).

47. Shan, Q., *et al.* Epigenetic modification of miR-10a regulates renal damage by targeting CREB1 in type 2 diabetes mellitus. *Toxicol Appl Pharmacol* **306**, 134–143 (2016).
48. Zocchi, L., *et al.* Scotin: A new p63 target gene expressed during epidermal differentiation. *Biochem Biophys Res Commun* **367**, 271–276 (2008).
49. Klöppel, G., Löhr, M., Habich, K., Oberholzer, M. & Heitz, P.U. Islet pathology and the pathogenesis of type 1 and type 2 diabetes mellitus revisited. *Surv Synth Pathol Res* **4**(**2**), 110–125 (1985).
50. Zhou, L., *et al.* Integrated profiling of microRNAs and mRNAs: microRNAs located on Xq27.3 associate with clear cell renal cell carcinoma. *PLoS One* **5**, e15224 (2010).
51. Zhang, X.F., Ou-Yang, L., Yang, S., Hu, X. & Yan, H. DiffNetFDR: differential network analysis with false discovery rate control. *Bioinformatics* **35**, 3184–3186 (2019).
52. Love, M.I., Huber, W. & Anders, S. Moderated estimation of fold change and dispersion for RNA-seq data with DESeq2. *Genome Biol* **15**, 550 (2014).
53. Xiao, X., *et al.* Pancreatic cell tracing, lineage tagging and targeted genetic manipulations in multiple cell types using pancreatic ductal infusion of adeno-associated viral vectors and/or cell-tagging dyes. *Nat Protoc* **9**, 2719–2724 (2014).
54. Tang, S., *et al.* Reversal of autoimmunity by mixed chimerism enables reactivation of beta cells and transdifferentiation of alpha cells in diabetic NOD mice. *Proc Natl Acad Sci U S A* **117**, 31219–31230 (2020).
55. Johnson, K.E., *et al.* Telemedicine-Based Health Coaching Is Effective for Inducing Weight Loss and Improving Metabolic Markers. *Telemed J E Health* **25**, 85–92 (2019).

Figures

Figure 1

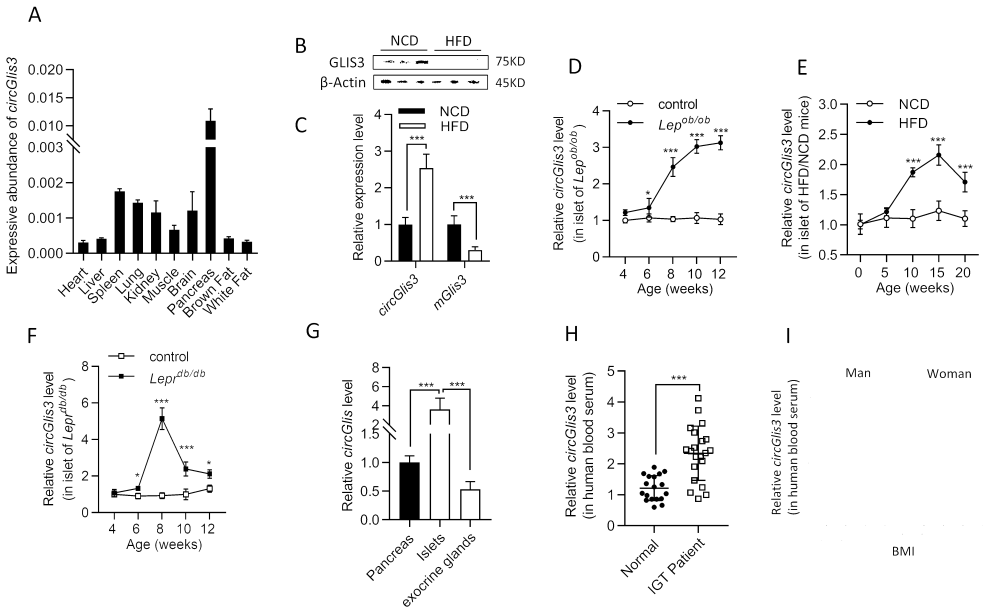

Figure 1

circGlis3 is upregulated in and is associated with obesity.

(A) qRT-PCR analysis of *circGlis3* expressive abundance, *circGlis3* is enriched in pancreas compared to that in other tissues (*n* = 3). (B) Western blot showing GLIS3 protein in pancreas of NCD- and HFD-fed mice (*n* = 3). (C) qRT-PCR analysis of *circGlis3* and *Glis3* mRNA in pancreas of NCD- and HFD-fed mice (*n*

= 3). (D) qRT-PCR analysis of *circGlis3* expression in the islets of *Lep*$^{ob/ob}$ mice aged from 4 to 12 weeks, HFD-fed mice from 0 to 20 weeks (E), and *Lepr*$^{db/db}$ mice aged from 4 to 12 weeks (F) (*n* = 6). (G) qRT-PCR analysis of *circGlis3* expression in primary islets and exocrine glands (*n* = 6). (H) qRT-PCR analysis of *circGlis3* expression in the sera of normal and impaired glucose tolerance human individuals (Normal *n* = 18, IGT patient *n* = 21). (I) Levels of *circGlis3* expression in the sera of human individuals with different BMI (Man *n* = 52, Woman *n* = 122). Data are represented as presented as the mean ± SEM. $^{*}p < 0.05$, $^{**}p < 0.01$, $^{***}p < 0.001$.

Figure 2

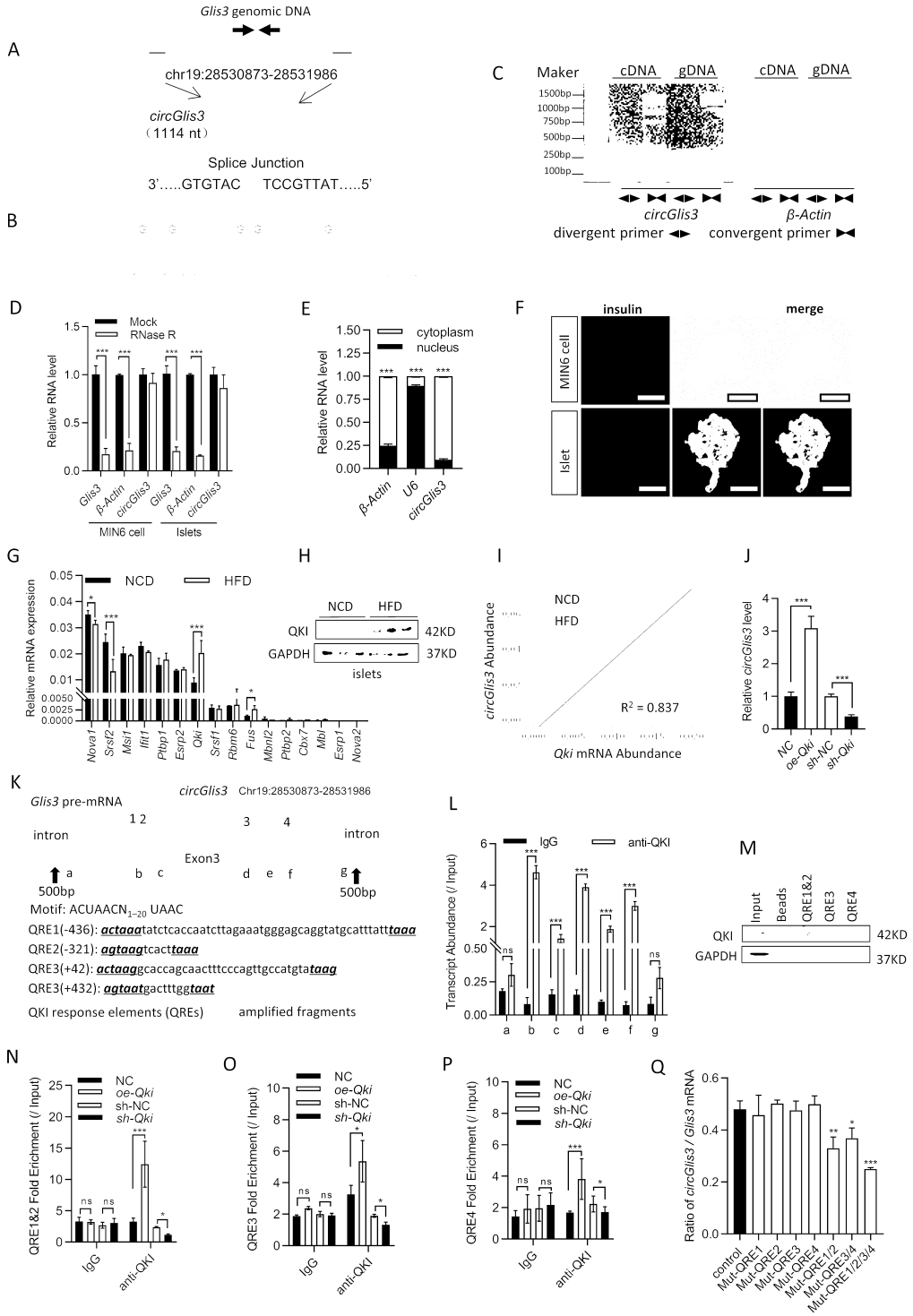

Figure 2

Identification of *circGlis3*, and splicing factor QKI regulates formation of *circGlis3*

(A) Circularization schematic of *circGlis3* derived from exon3 of host gene *Glis3.* (B) Sequencing analysis of head-to-tail splicing junction in *circGlis3*. (C) *circGlis3*, along with *β-Actin*, were amplified from cDNA or gDNA from MIN6 cells with divergent and convergent primers by PCR assays, respectively. (D) qRT-PCR

analysis of *circGlis3* and *β-Actin* mRNA levels in MIN6 cells and primary islets with and without RNase R treatment (n = 3). (E) Subcellular fractionation of MIN6 cells and measurement of *circGlis3* by qRT-PCR analysis (n =3). (F) FISH assay of *circGlis3* in MIN6 cells and primary islets (Red represents *circGlis3*, Green represents insulin, Blue represents DAPI). (G) Absolute quantification for various splicing factors in NCD and HFD islets were measured by qRT-PCR assays (n = 3). (H) Western blot showing QKI protein in NCD and HFD islets (n = 3). (I) The correlation of *circGlis3* and *Qki* mRNA abundance in NCD and HFD (n = 18) mice islets, respectively. (J) qRT-PCR analysis changes of *circGlis3* expression in MIN6 cells after QKI over-expressed and knocked-down (n = 3). (K) Schematic of *Glis3* pre-mRNA showing the locations of four putative QREs (inverted blue triangles) and amplicons (a-g) used for RIP assay, and sequence of QREs. Numbers in brackets refer to the distance from the *circGlis3* forming splice site. (L) Fold enrichment of endogenous *Glis3* intron fragments by QKI in MIN6 cells were detected by RIP and qRT-PCR, the qRT-PCR primers were designed and indicated in (K), n = 3. (M) Biotin-labeled probes of *Glis3* intron fragments containing QREs were used for RNA-QKI pull-down against MIN6 cell lysates, and western blot results showing QKI was pulled down. (N-P) RIP and qRT-PCR assays were used to evaluate that QKI expression levels effected the binding interaction between *circGlis3* and motif sites (QRE1&2, QRE3, QRE4) (n = 3). (Q) Effect of mutations to the QREs on the ratio of circRNA to linear mRNA, as determined by ratios of Absolute quantification by qRT-PCR assays (n = 3). Data are represented as presented as the mean ± SEM. $^{*}p < 0.05$, $^{**}p < 0.01$, $^{***}p < 0.001$.

Figure 3

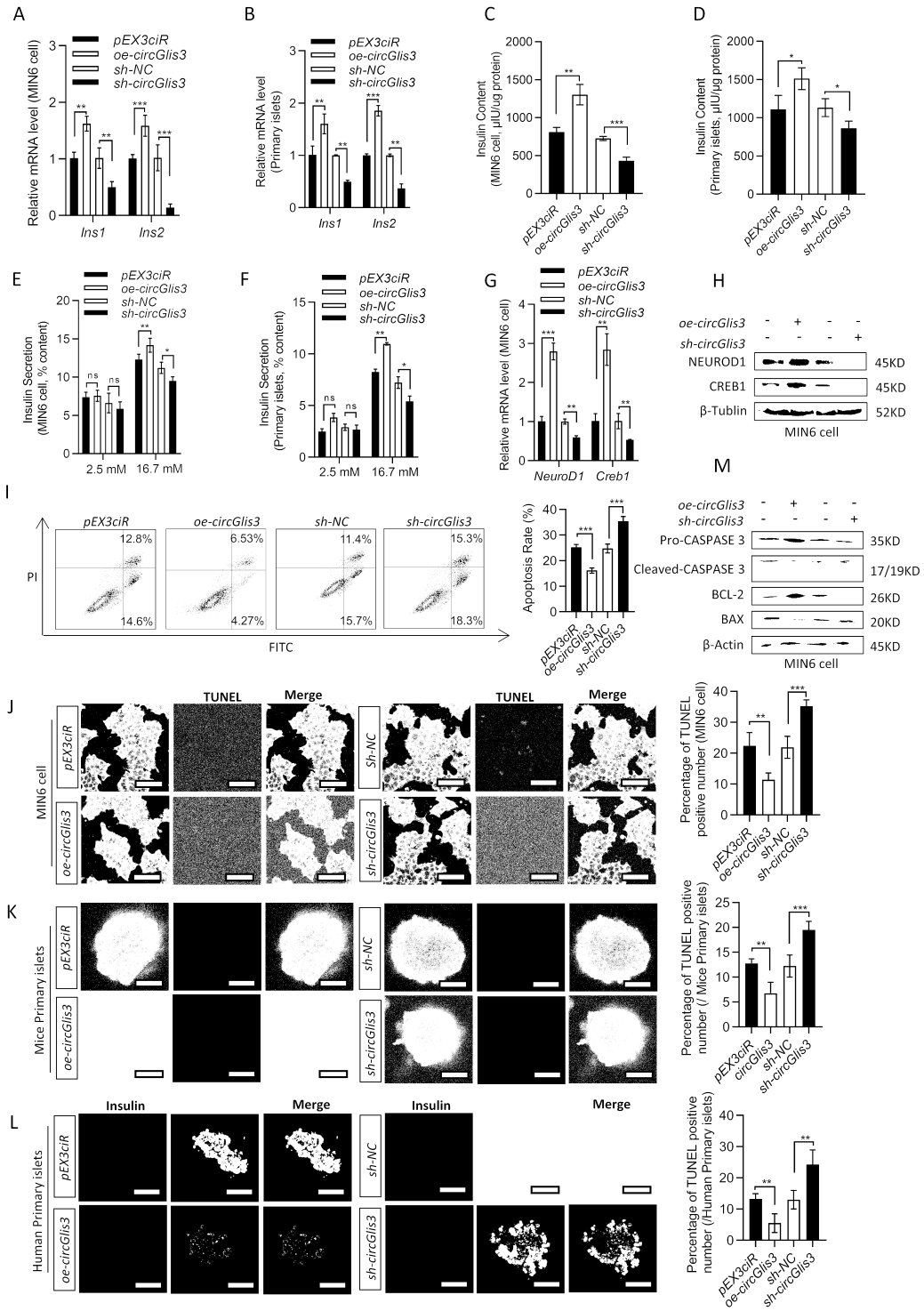

Figure 3

Upregulation of circGlis3 promotes insulin transcription and secretion and inhibits β-cell apoptosis *in vitro*.

(A-B) qRT-PCR analysis of expression of *Ins2* and *Ins2* mRNA after *circGlis3* over-expressed and knocked-down in MIN6 cells and mice primary islets (*n* = 3). (C-D) Insulin content of MIN6 cells and mice primary

islets after *circGlis3* over-expressed and knocked-down (*n* = 3). (E-F) Insulin secretion in glucose (2.5 mM and 16.7 mM) stimulated MIN6 cells and mice primary islets after *circGlis3* over-expressed and knocked-down (*n* = 3). (G) qRT-PCR analysis of expression of *NeuroD1* and *Creb1* mRNA in MIN6 cells after *circGlis3* over-expressed and knocked-down (*n* = 3). (H) Western blot showing NEUROD1 and CREB1 protein in MIN6 cells after *circGlis3* over-expressed and knocked-down. (I) Annexin V/PI staining and flow cytometry analysis of cell apoptosis in MIN6 cells after *circGlis3* over-expressed and knocked-down (*n* = 3). (J) TUNEL assays and statistic results of cell apoptosis in MIN6 cells (Red represents Insulin, Green represents positive TUNEL cells; Scale bars represent 50 μm), primary mice islets (Red represents Insulin, Green represents positive TUNEL cells; Scale bars represent 100 μm) (K), and primary human islets (Red represents positive TUNEL cells, Green represents Insulin; Scale bars represent 100 μm) (L) after *circGlis3* over-expressed and knocked-down, respectively. (M) Western blot showing Pro-CASPASE-3, Cleaved-CASPASE-3, BAX and BCL-2 proteins in MIN6 cells with *circGlis3* over-expressed and knocked-down Data are represented as presented as the mean ± SEM. $^{*}p < 0.05$, $^{**}p < 0.01$, $^{***}p < 0.001$.

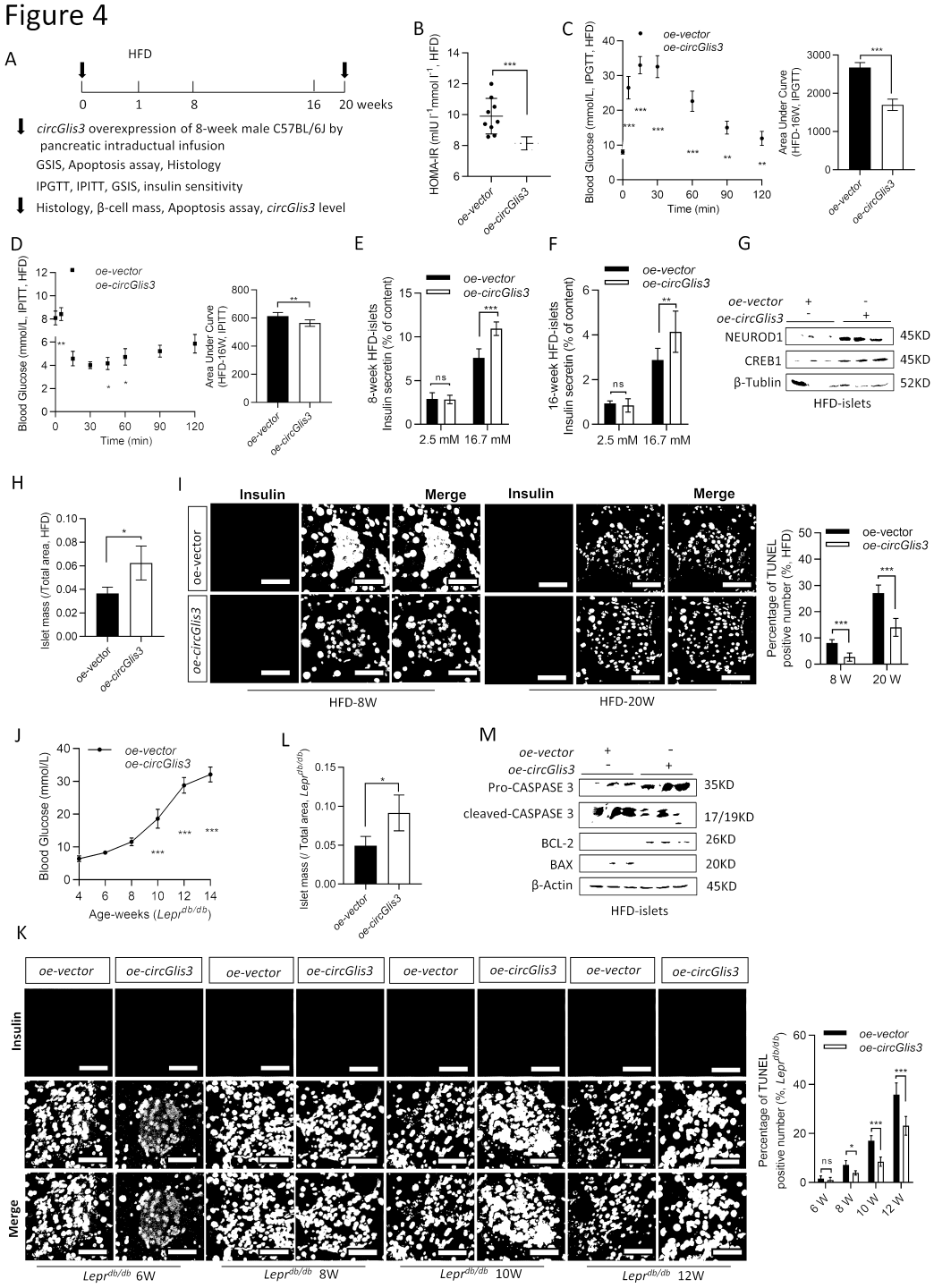

Figure 4

Overexpression circGlis3 protects against β-cell dysfunction and apoptosis *in vivo*.

(A) Flowchart of the in vivo experiments designed for detecting β-cell function via pancreatic ductal infusion (n = 10^{-12}), 8-week-old male mice (adeno-associated virus serotype 8 vector (AAV8)-MIP (Mouse Insulin1 promoter)-*circGlis3*) were exposed to HFD for 20 weeks. (B) HOMA-IR at indicated time points of

circGlis3 over-expressed mice with HFD-fed compared with control mice (n = 6). HOMA-IR was calculated as HOMA-IR= (FBG (mmol/L) x FINS (mIU/L))/22.5. (C-D) Intraperitoneal glucose tolerance test (IPGTT) (2 g/kg) and Intraperitoneal insulin tolerance test (IPITT) (1 U/kg) performed in overnight fasted mice with *circGlis3* over-expressed after 12-week of HFD feeding (n = 6). The corresponding area under the curve (AUC) was calculated. (E-F) Insulin secretion in glucose (2.5 mM and 16.7 mM) stimulated islets from mice with *circGlis3* over-expressed and HFD-fed for 8 weeks and 16 weeks (n = 6). (G) Western blot showing NeuroD1 and Creb1 protein expression in mice with *circGlis3* over-expressed (n = 3). (H) Islet mass of mice with *circGlis3* over-expressed and HFD-fed (n = 6). (I) TUNEL assays and statistic results of pancreatic sections from negative control and *circGlis3* over-expressed mice with HFD-fed for 8 weeks and 20 weeks (Red represents positive TUNEL cells, Green represents Insulin; Scale bars represent 100 μm). (J) Fasting blood glucose in $Lepr^{db/db}$ mice with *circGlis3* over-expressed at age from 4 to 12 weeks (n = 6). (K) TUNEL assays and statistic results of pancreatic sections from $Lepr^{db/db}$ mice at age from 6 to 12 weeks (Red represents positive TUNEL cells, Green represents Insulin; Scale bars represent 50 μm). (L) Islet mass of $Lepr^{db/db}$ mice with *circGlis3* over-expressed (n = 6). (M) Western blot showing Pro-Caspase-3, Cleaved-CASPASE 3, BAX and BCL-2 proteins in islets from mice with *circGlis3* over-expressed (n = 3). Data are represented as presented as the mean ± SEM. $^{*}p < 0.05$, $^{**}p < 0.01$, $^{***}p < 0.001$.

Figure 5

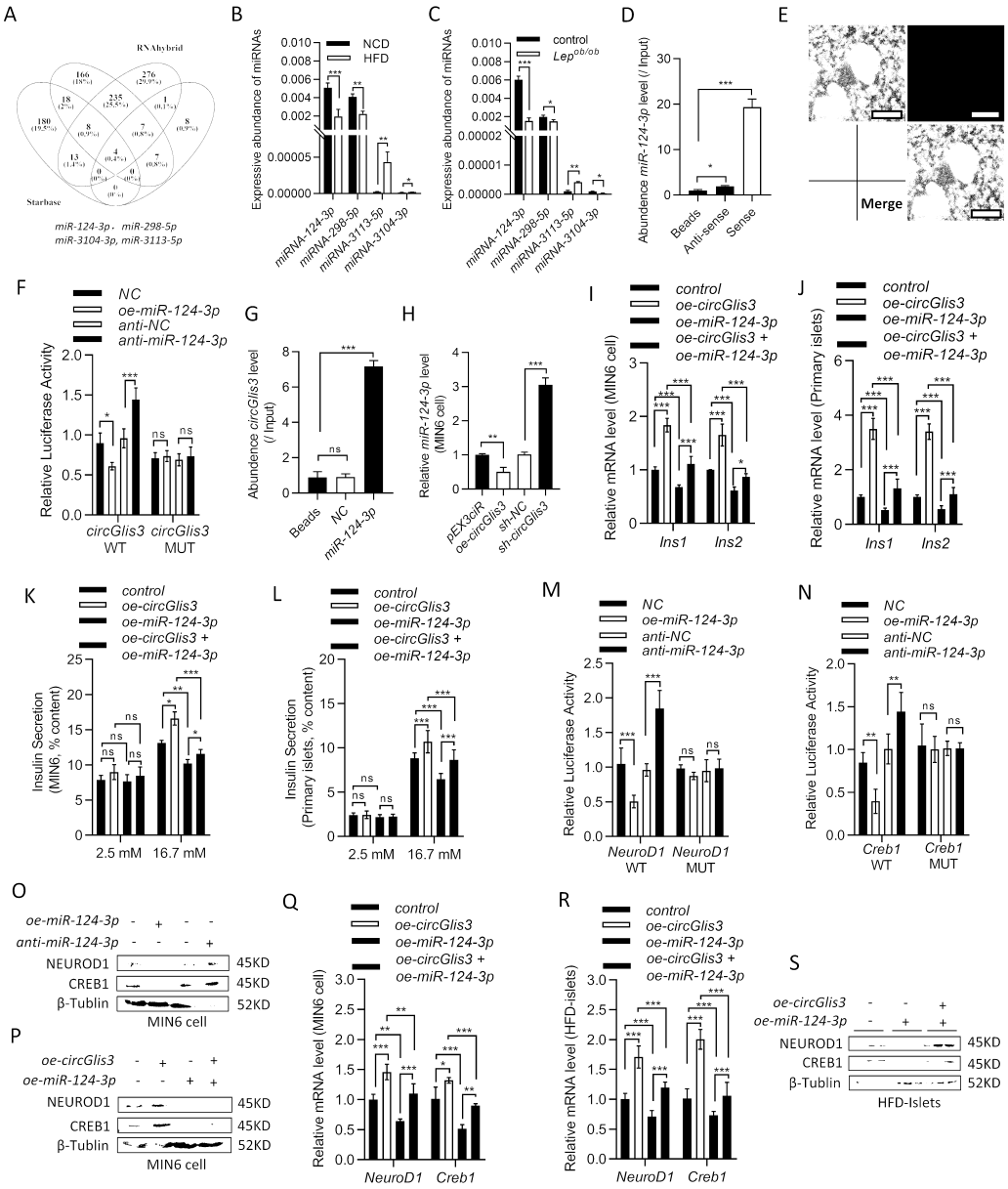

Figure 5

circGlis3 regulates insulin transcription by targeting and sponging *miR-124-3p*

(A) Schematic illustration showing the overlap of the target miRNAs of *circGlis3* predicted by miRanda, RNAhybrid, Starbase and Targetscan. (B-C) The relative levels of four miRNA candidates in islets from HFD-fed mice and *Lep*$^{ob/ob}$ mice were detected by RT-qPCR (n = 3). (D) RNA pull-down and RT-qPCR assay

showed that the amount of endogenous *miR-124-3p* pulled down by beads binding with biotin-labeled *circGlis3* sense or anti-sense (*n* = 3). (E) Co-localization between *miR-124-3p* and *circGlis3* in MIN6 cells by FISH assays (Red represents *circGlis3*, Green represents *miR-124-3p,* Scale bars represent 20 μm). (F) *circGlis3*-WT and *circGlis3*-MUT sequence were cloned into the 3′-UTR of the pMIR-REPORT Luciferase reporter, and transfection *miR-124-3p* mimic repressed the reporter activity of pMIR-*circGlis3*-WT, and such repression could be restored by *anti-miR-124-3p* (*n* = 3). (G) RNA pull-down and RT-qPCR assay showed that the amount of endogenous *circGlis3* pulled down by biotin-labeled *miR-124-3p* (*n* = 3). (H) qRT-PCR analysis of *miR-124-3p* expression in MIN6 cells after *circGlis3* over-expressed and knocked-down (*n* = 3). (I-J) qRT-PCR analysis of *Ins1* and *Ins2* mRNA expression in *circGlis3* and *miR-124-3p* over-expressed MIN6 cells (*n* = 3) and islets from *circGlis3* and *miR-124-3p* over-expressed mice (*n* = 6). (K-L) Insulin secretion in *circGlis3* and *miR-124-3p* over-expressed MIN6 cells (*n* = 3) and islets from mice with *circGlis3* and *miR-124-3p* over-expressed (*n* = 6). (M-N) Relative luciferase activity of the pMIR-REPORT constructs containing either the wild type or mutated 3′-UTR of the *NeuroD1* and *Creb1* gene (*n* = 3). (O) Western blot showing NEUROD1 and CREB1 protein expression in MIN6 cells transfected with *miR-124-3p* mimics and inhibitors. (P-Q) Western blot results and qRT-PCR analysis showing *NeuroD1* and *Creb1* mRNA and protein expression in MIN6 cells with *circGlis3* and *miR-124-3p* over-expressed (*n* = 3). (R-S) qRT-PCR analysis and western blot results of *NeuroD1* and *Creb1* mRNA and protein expression in islets from mice with *circGlis3* and *miR-124-3p* over-expressed (*n* = 3). Data are represented as presented as the mean ± SEM. $^{*}p < 0.05$, $^{**}p < 0.01$, $^{***}p < 0.001$.

Figure 6

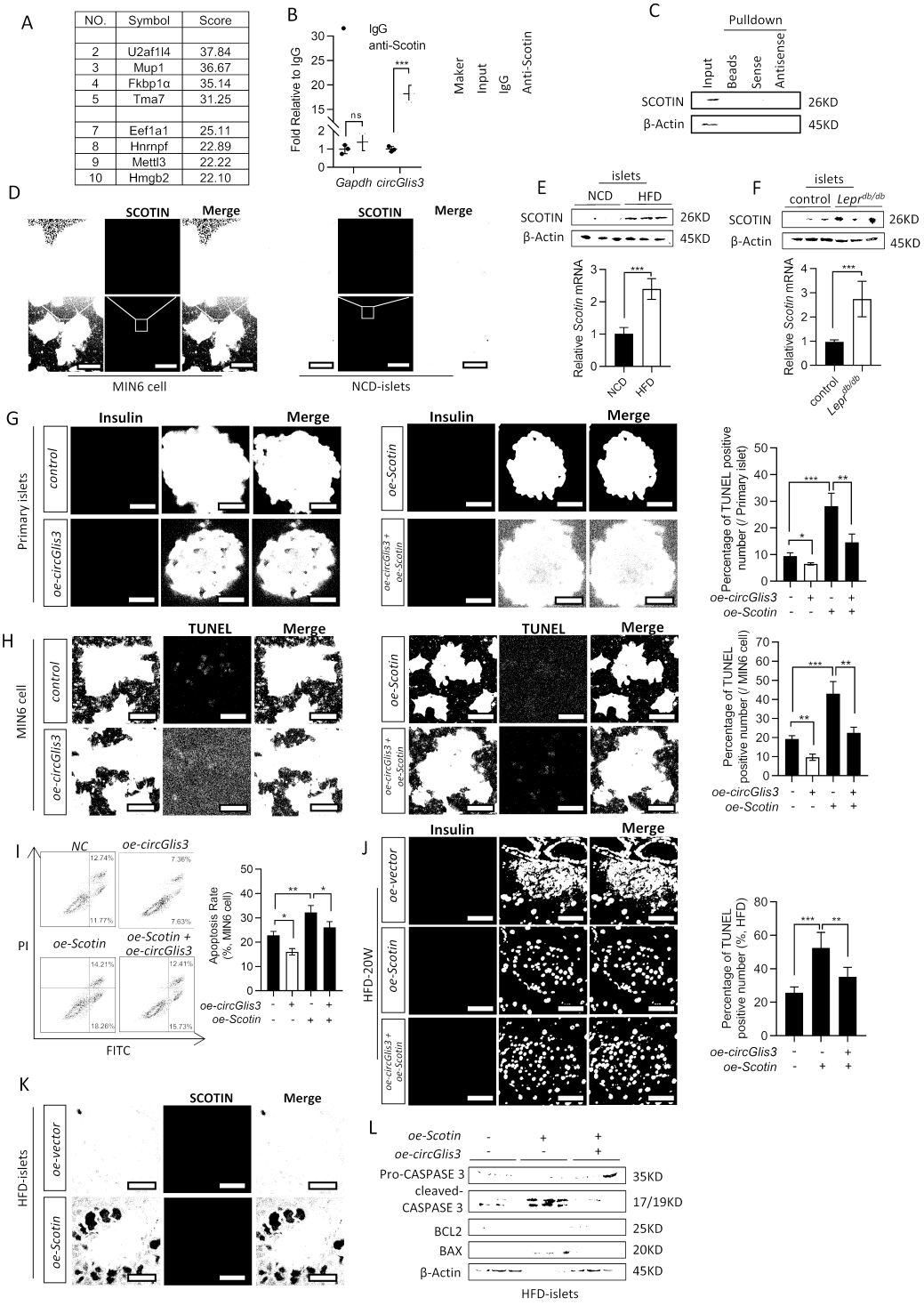

Figure 6

circGlis3 prevents β-cell apoptosis by directly binding to SCOTIN

(A) The mass spectrometry assay revealing the proteins (score > 20 by Mascot Software) pulled down by biotin-labeled *circGlis3* from the lysates of MIN6 cells. (B) Fold enrichment of endogenous *circGlis3* by SCOTIN in MIN6 cells were detected by RIP and qRT-PCR (*n* = 3). (C) Biotin-labeled sense or antisense

circGlis3 probes were used for *circGlis3*-protein pull-down against MIN6 cell lysates, and western blot results showing SCOTIN was pulled down. (D) Co-localization between *circGlis3* and SCOTIN in MIN6 cell (Red represents *circGlis3*, Green represents SCOTIN, Scale bars represent 50 μm) and pancreas sections (Scale bars represent 100 μm) by circFISH and Immunofluorescence assays. (E-F) qRT-PCR analysis and western blot results of *Scotin* mRNA and protein expression in islets from HFD-fed mice and $Lepr^{db/db}$ mice ($n = 3$). (G-H) TUNEL assays and statistic results of primary mice islets (Red represents positive TUNEL cells, Green represents Insulin; Scale bars represent 100 μm) and MIN6 cells (Red represents Insulin, Green represents positive TUNEL cells; Scale bars represent 50 μm) with *circGlis3* and *Scotin* over-expressed. (I) Annexin V/PI staining and flow cytometry analysis of cell apoptosis in MIN6 cells with *circGlis3* and *Scotin* over-expressed ($n = 3$). (J) TUNEL assays and statistic results of pancreatic sections from mice with *circGlis3* and *Scotin* over-expressed and HFD-fed for 20 weeks (Red represents positive TUNEL cells, Green represents Insulin; Scale bars represent 100 μm). (K) Immunofluorescence assays showing overexpression of SCOTIN induces sequestration of *circGlis3* in the cytoplasm (Red represents *circGlis3*, Green represents SCOTIN; Scale bars represent 100 μm). (L) Western blot showing Pro-CASPASE 3, Cleaved-CASPASE 3, BAX and BCL-2 proteins in islets from mice with *circGlis3* and *Scotin* over-expressed ($n = 3$). Data are represented as presented as the mean ± SEM. $^{*}p < 0.05$, $^{**}p < 0.01$, $^{***}p < 0.001$.

Figure 7

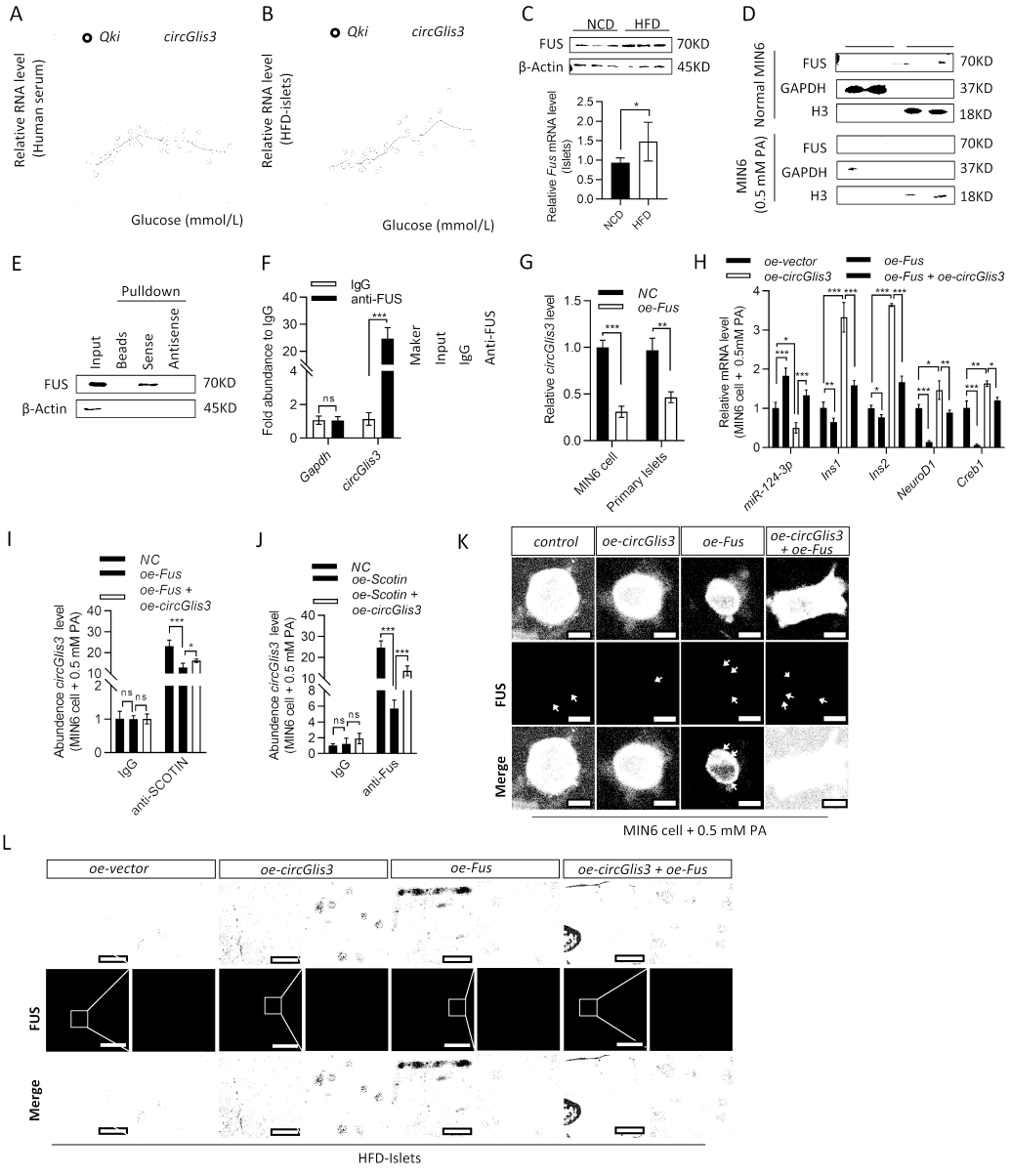

Figure 7

FUS sequestrates *circGlis3* to reduce its abundance in diabetes by assembling cytoplasmic SGs

(A-B) Correlation analysis of the expression of *circGlis3* and *Qki* mRNA in patients with impaired glucose tolerance or T2DM (*n* = 55) and in mice with HFD-fed (*n* = 40). (C) Western blot showing FUS protein expression in islets from NCD mice and HFD mice (*n* = 3). (D) Western blot showing FUS shuttle between

the nucleus and cytoplasm in responses to palmitate stress in MIN6 cells. (E) Biotin-labeled sense or antisense *circGlis3* probes were used for RNA-protein pull-down against MIN6 cell lysates, and western blot results showing FUS was pulled down. (F) Fold enrichment of endogenous *circGlis3* by FUS in MIN6 cells were detected by RIP and qRT-PCR ($n = 3$). (G) qRT-PCR analysis of *circGlis3* expression in MIN6 cells and primary islets with *Fus* over-expressed ($n = 3$). (H) qRT-PCR analysis of *miR-124-3p, Ins1, Ins2, NeuroD1* and *Creb1* mRNA in MIN6 cells with *Fus* and *circGlis3* over-expressed ($n = 3$). (I) RIP and qRT-PCR assay analyze fold enrichment of endogenous *circGlis3* by SCOTIN in palmitate stimulated MIN6 cells with *Fus* over-expressed ($n = 3$). (J) RIP and qRT-PCR assay analyze fold enrichment of endogenous *circGlis3* by FUS in palmitate stimulated MIN6 cells with *Scotin* over-expressed ($n = 3$). (K-L) circFISH and Immunofluorescence assays of palmitate stimulated MIN6 cells (Red represents *circGlis3*, Green represents FUS; Scale bars represent 20 μm) and pancreas sections from HFD-fed mice (Red represents *circGlis3*, Green represents FUS; Scale bars represent 100 μm) to detect co-location between *circGlis3* and FUS in SGs. Data are represented as presented as the mean ± SEM. $^{**}p < 0.01$, $^{***}p < 0.001$.

Figure 8

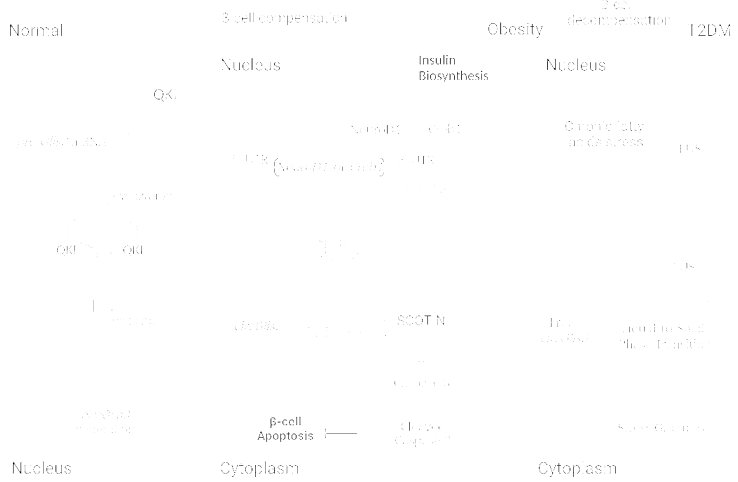

Figure 8

A working model that illustrates the mechanism by which *circGlis3* regulates β-cell function.

circGlis3 is regulated by QKI-mediated splicing and increases in obese and moderately diabetic individuals, while it decreases when diabetes occurs via FUS-formed SGs. *circGlis3* functions in β-cell

compensation through regulating insulin transcription and apoptosis by sponging *miR-124-3p* and directly binding SCOTIN provide a potential therapeutic angle.

Supplementary Files

This is a list of supplementary files associated with this preprint. Click to download.

- SupplementalTables.pdf
- gelsandblots.pdf
- figureS1.tif
- figureS2.tif
- figureS3.tif
- figureS4.tif
- figureS5.tif
- figureS6.tif
- figureS7.tif